



Cite this: *RSC Appl. Polym.*, 2025, **3**, 532

Received 29th November 2024,  
Accepted 2nd February 2025

DOI: 10.1039/d4lp00351a  
[rsc.li/rscapplpolym](http://rsc.li/rscapplpolym)

## Smart inhibitor systems towards anti-corrosion: design and applications

Danping Li,<sup>a</sup> Ziwen Zhang,<sup>a</sup> Bilegsaikhan Sukhbat,<sup>a</sup> Xuejie Wang,<sup>a</sup> Xue Zhang,<sup>b</sup> Jing Yan,<sup>a\*</sup> Junping Zhang,<sup>a</sup> Qiuyu Zhang,<sup>a</sup> Yan Li,<sup>c</sup> Hao Wang<sup>d</sup> and Yi Yan <sup>a</sup>

Smart corrosion inhibitor systems have been a hot research topic in recent years. Compared with conventional corrosion inhibitors or coatings, corrosion inhibitors can be released according to specific tasks to achieve more precise corrosion protection for metals. Such smart inhibitor systems are generally based on environmental stimuli such as pH, light, ions, etc., which save the cost of corrosion inhibitors and additives, and therefore improve the effectiveness of corrosion inhibition applications. Herein, the research progress on smart corrosion inhibitors in the past decade will be summarized, including the design, synthesis, smart release, and applications of different smart inhibitor systems.

## 1 Introduction

Corrosion inhibitors, as one of the important solutions for industrial anti-corrosion, have received broad attention in both industry and academia.<sup>1–3</sup> They offer the advantages of simple implementation, quick effectiveness, and high cost-efficiency. Organic corrosion inhibitors primarily form protective films through either physical or chemical adsorption, whereas inorganic corrosion inhibitors mainly create precipitation films and oxide films. Compared with anti-corrosion measures such as corrosion-resistant materials and coatings, the use of corrosion inhibitors is consumable and requires a continuous supply, which increases the cost and time associated with manual operations.<sup>4–7</sup> Since conventional corrosion inhibitors cannot smartly respond to changing corrosion environments, there is a need to develop a smart response corrosion inhibitor system that can target specific areas and enhance protection, thereby improving the utilization rate and effectiveness of the inhibitor,<sup>8,9</sup> which is referred to as a smart inhibitor in this paper. Meanwhile, the synergistic effect between corrosion inhibitors and coatings has also been a focus of research in recent years. The use of corrosion inhibitors to repair damaged areas of coatings and form self-healing

coatings addresses the problem of endless monitoring and manual repairs following coating failures such as blistering and peeling, which are time-consuming and resource-intensive.<sup>10</sup> However, in different coating systems, conventional corrosion inhibitors that are loaded directly have several drawbacks, such as: (i) a slow or uncontrollable release rate; (ii) the high solubility of corrosion inhibitors, which can lead to blistering and delamination of protective coatings; and (iii) the semi-permeable membrane, which allows for the transportation of water, causing damage to the barrier layer. If the corrosion inhibitor is coated with environmentally sensitive materials<sup>11–17</sup> or carried by a carrier,<sup>8,16,18–20</sup> and then loaded into the coating, when local corrosive environmental conditions, such as pH, ion exchange, or temperature, change,<sup>16,21</sup> the corrosion inhibitor will automatically release,<sup>22–24</sup> inhibiting or slowing down the occurrence of corrosion. It achieves the purpose of in-service repair of the coating, while improving the utilization rate of the corrosion inhibitor and reducing the manufacturing and maintenance costs of the coating.<sup>25,26</sup>

Different host materials can be used to construct smart inhibitor systems. For example, mesoporous silica nanocarriers (MSN) were used to encapsulate benzotriazole (BTA) to create a multifunctional smart coating known as ACR-MSN-BTA-Ag. This coating has a dual anti-corrosion mechanism under aggressive conditions involving  $\text{Cl}^-$ : a passive mechanism based on a pH-responsive BTA-Ag complex that triggers the release of BTA to form a protective layer adsorbed on the metal surface. Another active mechanism is attributed to the ability of silver ions to trap chloride ions. In pH 1.5 hydrochloric acid vapor, the ACR-MSN-BTA-Ag smart coating showed an excellent anti-corrosion effect compared with the ACR coating and the ACR-BTA coating.<sup>27</sup> pH change can stimulate the release of  $\text{Ce}(\text{III})$  from a PANI– $\text{Ce}(\text{III})$

<sup>a</sup>Department of Chemistry, School of Chemistry and Chemical Engineering, Key Laboratory of Special Functional and Smart Polymer Materials of Ministry of Industry and Information Technology, Northwestern Polytechnical University, Xi'an, Shaanxi, 710129, China. E-mail: [yanyi@nwpu.edu.cn](mailto:yanyi@nwpu.edu.cn), [yanjing@nwpu.edu.cn](mailto:yanjing@nwpu.edu.cn)

<sup>b</sup>Chengdu Aircraft Industrial (Group) Co., Ltd., China

<sup>c</sup>Petroleum Technology Research Institute, Tarim Oilfield Company, Petrochina, Korla, Xinjiang 841000, China

<sup>d</sup>The First Gas Production Plant, Changqing Oilfield Company, Yulin, Shaanxi 718500, China



complex. Najibzad *et al.*<sup>28</sup> prepared praseodymium cation and PANI composites, which were then added to silane coatings applied to magnesium alloys. They found that coatings containing praseodymium cation and PANI composites exhibited better corrosion resistance and self-healing properties than those containing only praseodymium nitrate. Introducing  $\text{TiO}_2/\text{PANI}-\text{MoO}_4^{2-}/\text{PDA}$  nanocontainers into smart waterborne epoxy (WEP) coatings, the charge transfer resistance increases by a factor of  $3.32 \times 10^5$  compared with that of WEP coatings.<sup>29</sup> The inhibitor was encapsulated into HNTs using a vacuum method, and another inhibitor, dodecylamine (DDA), was intercalated into the polyelectrolyte multilayer film using a layer technique to form HHNTs. The HHNTs (3 wt%) were then sufficiently dispersed into the epoxy resin matrix to develop a smart blend self-healing polymer coating known as a blend coating. It exhibits active release in both acidic and alkaline media, making it suitable for protecting steel in the early stages of coating damage, while DDA is effectively released in acidic media, which may help prevent corrosion activity in the later stages of coating deterioration.<sup>30</sup> Polydopamine (PDA) is used as a pH-sensitive gating material that exhibits rapid release in acidic environments. The on-demand release of PDA and  $\text{La}^{3+}$  corrosion inhibitors at the scratch site increased the total corrosion resistance (RT) of the carbon nanofiber (CNF) coating containing modified PDA-La(m) composite by 117% in brine compared with the blank epoxy.<sup>31</sup> Multifunctional dopamine-based gating materials not only have potential applications in smart self-healing anti-corrosion coatings, but they can also be used in drug delivery, antimicrobial protection, and other fields.<sup>32</sup>

Metal-organic frameworks (MOFs) can also be used as host materials. For example, stimulus-responsive zeolite imidazole framework was developed and subsequently applied to sense local corrosion and restore the protective effect of polymer coating systems. The change in local pH value and the occurrence of metal corrosion due to coating micro-defects can be sensed and indicated in real-time by the released tannic acid, which provides an obvious color signal. In addition, the decomposition of the ZIF-7@PEG-TA nanosensor produces abundant corrosion inhibitors, allowing the formation of an inhibition layer that can significantly reduce the spread of interface corrosion reactions and actively contribute to anti-corrosion functions.<sup>33</sup> Triple-functional microcarriers with corrosion sensing, self-healing, and anti-corrosion capabilities were developed and embedded in the coating to detect color changes and the release of corrosion inhibitors when the local pH near the metal surface changes due to the formation of hydroxide ions during the corrosion process. It significantly reduces the corrosion rate of the coated metal.<sup>34</sup> The anodic peak corresponding to the corrosion point of the mechanical defect on the surface of the photosensitive coating prepared with  $\text{TiO}_2$  disappeared immediately after irradiation with a layer of polyethylene imide (PEI) and polystyrene sodium sulfonate (PSS).<sup>35,36</sup> After soaking in a 0.5 M NaCl solution for 2 weeks, the total impedance of the PVB coating decreased from  $1 \text{ m}\Omega \text{ cm}^2$  to  $20 \text{ k}\Omega \text{ cm}^2$ , while the coating containing the

$\text{Zn}_2\text{Fe}(\text{CN})_6$  ion-exchange smart corrosion inhibitor remained basically unchanged at  $15 \text{ m}\Omega \text{ cm}^2$ , demonstrating excellent anti-corrosion properties.<sup>37</sup> When polyurea formaldehyde was embedded in BTA and magnetic multi-wall carbon nanotubes and combined with the coating, the corrosion inhibition rate reached 91.2%, and the self-healing efficiency was 6.4 times greater than that of non-magnetic self-healing coatings.<sup>38</sup> By adding pH-responsive thiourea-containing nanovessels to the ethylcellulose coating, the rate of thiourea release is increased once stimulated by  $\text{CO}_2$ . The response structure significantly improves the corrosion resistance of the coating in 3.5 wt% NaCl solution with and without  $\text{CO}_2$ .<sup>39</sup> In summary, the smart repair of coatings depends on the use of smart corrosion inhibitors.

Some pioneers in this field have already summarized the progress of smart corrosion inhibitor systems. Abu-Thabit *et al.*<sup>40</sup> reviewed the research progress in using polyelectrolyte multilayer films as stimulus-responsive materials to prepare coatings with smart self-healing function in recent years. The novelty of PEMs lies in their ability to provide responsive actions based on various triggering mechanisms of the surrounding environment. The advantage of using PEMs lies in the versatility of layer-by-layer (LbL) assembly, which can be used to prepare PEMs for various planar, non-planar, and granular substrates. Cai *et al.*<sup>10</sup> reviewed the research progress of smart anti-corrosion coatings based on stimulus-responsive micro-nano-containers, introduced the latest design and manufacturing technologies of micro-nano-containers, and provided detailed examples. M. Samadzadeh *et al.*<sup>41</sup> reviewed the effective parameters for the synthesis of micro/nanocapsules, several methods for preparing self-healing coatings based on micro/nanocapsules, and the drawbacks of embedding micro/nanocapsules in coating matrices. Rowsell *et al.*<sup>42</sup> reviewed the synthesis, structure, and properties of metal-organic frameworks (MOFs), as well as their selective absorption of small molecules and optical or magnetic response to objects. Guo *et al.*<sup>43</sup> reviewed pH-responsive and ion exchange-based smart corrosion inhibitors. By introducing cobaltocenium groups to the polymer, we designed a series of metallo-polyelectrolytes and metallo-surfactants, which exhibited robust anti-corrosion performance.<sup>44-46</sup> Based on our previous review article on the polymeric inhibitor,<sup>47</sup> we herein are trying to summarize the most recent research progress on the response mechanism and smart response structure of smart corrosion inhibitor systems, including pH, light, ion, magnetic, temperature and redox responsive as well as multiple-responsive systems.

## 2 General mechanisms of smart inhibitor systems

To achieve the controlled release of inhibitors under different conditions, several smart inhibitor systems have been developed. In this section, the general mechanisms of smart inhibitor systems will be discussed, including pH-responsive, photo-responsive, ion-responsive, and other systems.



## 2.1 Mechanism of pH-responsive inhibitor systems

Generally, electrochemical corrosion consists of anodic and cathodic reactions, resulting in an acidic environment in the anode region and alkaline condition in the cathode region. Therefore, a pH-responsive corrosion inhibitor system presents an optimal strategy for mitigating electrochemical corrosion. In principle, these pH-responsive inhibitor systems are designed to release inhibitors in response to pH changes, effectively inhibiting both anodic and cathodic corrosion to achieve the desired anti-corrosion performance. As shown in Fig. 1, there are mainly four types of pH-responsive inhibitor system, namely inhibitors encapsulated in polyelectrolyte capsules, pH-sensitive capsule wall, nanovalve type, and carrier grafting *via* chemical bonds.

A polyelectrolyte microcapsule is usually fabricated *via* a core-template approach, wherein polyelectrolytes with opposite charges are sequentially deposited on the core. These microcapsules can be categorized into two types according to the different core: (i) a sacrificial core, such as a  $\text{CaCO}_3$  particle, which can be dissolved after the formation of the microcapsules; and (ii) a mesoporous core that can be used to encapsulate corrosion inhibitors, such as silica, cerium oxide, carbon hollow spheres (CHSs), and halloysite nanotubes (HNTs). The inhibitors may either be encapsulated in the microcapsules or dispersed between the polyelectrolyte layers. Upon corrosion, the pH changes in either the anode or the cathode region may disrupt the overall charge equilibrium and swell the polyelectrolyte shell to release corrosion inhibitors into the solution. In most case, such a process is reversible.

In the case of type 2, the shell of the microcapsule is doped with pH-sensitive components, which may undergo chemical reactions upon a pH change, leading to the formation of pores

in the shell, and therefore, the release of the corrosion inhibitor. The chemical reactions used in this system involve ether bonds, ester bonds, disulfide groups, sulfhydryl groups, and so on.<sup>48</sup>

Besides microcapsules, the nanovalve system can also be used to construct smart inhibitor systems. The nanovalve system is usually composed of a micro-container for inhibitors and a pH-responsive cap. For example, macrocycles such as cucurbituril and its analogues can be used as a cap, while porous materials such as mesoporous silica, halloysite nanotubes and carbon hollow spheres are typically used as micro-containers.

Another method for preparing a pH-responsive inhibitor system involves grafting inhibitors onto the carrier surface *via* covalent bonds. In this case, 2D nanomaterials such as MXenes and 3D metal-organic frameworks (MOFs) can serve as the carriers. The pH response is achieved by functionalizing the surface of the carrier. For instance, the modification of the surface of MXene with  $-\text{NH}_2$  and subsequent protonation under acidic conditions will result in the release of corrosion inhibitors.<sup>49,50</sup> Additionally, acid-sensitive spacers can be used to graft inhibitors onto the polymer framework. The acid-sensitive linker used in this system include orthoesters, acetals, imines, *cis*-ketoacyls, vinyl ethers, silyl ethers, hydrazine groups, and  $\beta$ -thiopropionate groups.<sup>51</sup>

## 2.2 Mechanism of photoresponsive inhibitor systems

Owing to its green characteristic and remote control capabilities, a photoresponsive system can also be used to achieve the controlled release of corrosion inhibitors through the following strategies: photothermal effect from metal oxide/noble metal nanoparticles, photoisomerization or photooxidation, star polyelectrolytes, and photosensitive dyes (Fig. 2).

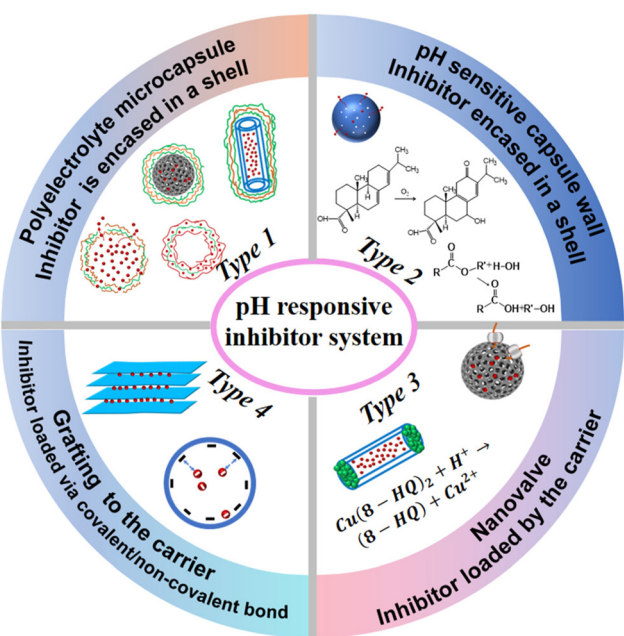


Fig. 1 Typical types of pH-responsive corrosion inhibitor system.

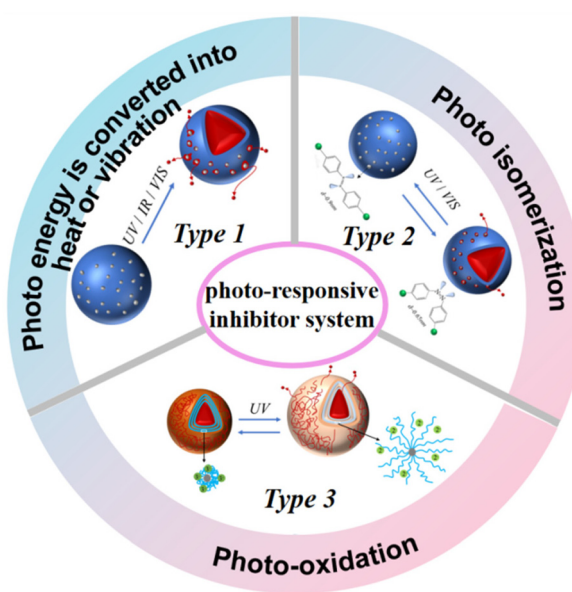


Fig. 2 Typical types of photoresponsive corrosion inhibitor system.



Metal oxide and noble metal nanoparticles, such as  $\text{TiO}_2$ ,<sup>20,52</sup> silver,<sup>53</sup> gold,<sup>54,55</sup> and gold-sulfide clusters,<sup>56</sup> possess the capacity to absorb light and convert it to thermal energy. By incorporating these nanoparticles into microcapsules, the photothermal effect can disrupt the shell of the microcapsule and lead to the release of the corrosion inhibitor (Fig. 2 Type 1). For example, in the case of  $\text{TiO}_2$ -containing microcapsules, the electron density of  $\text{TiO}_2$  can be altered through UV irradiation, while the decomposition of polyelectrolyte capsules is facilitated by the photocatalysis of  $\text{TiO}_2$  in the inorganic layer. The potential toxicity of metal nanoparticles, coupled with their elevated cost, may constrain their application in certain domains.

Microcapsules with photoisomerization units<sup>57</sup> can also be used in the controlled release of inhibitors. Owing to its abundant chemistry and reversible photoisomerization, azobenzene is widely used in the design of photoresponsive microcapsules (Fig. 2 Type 2). Under UV stimulation, the permeability of microcapsules can change from the stable *trans* form to the unstable *cis* form, allowing for the release of the encapsulated corrosion inhibitor.

Units that undergo photochemistry, such as photo-oxidation,<sup>58</sup> can also be used to construct photoresponsive inhibitor systems (Fig. 2 Type 3). For example, the photoaquation reaction of hexacyanocobaltate(III) ions provides a reversible change between  $\text{Co}(\text{CN})_6^{3-}$  and  $\text{Co}(\text{CN})_5(\text{H}_2\text{O})^{2-}$ , resulting in the collapse and swelling of the microcapsule, respectively. Such reversible transition can be used to control the release of inhibitors.<sup>59</sup> Moreover, specific dyes that absorb or emit light within the visible spectrum can be engineered into photosensitive microcapsules. These capsules incorporate elements such as fluorescent and functional dyes,<sup>60</sup> which react to either visible light or infrared radiation. Upon exposure to suitable light, alterations occur in the permeability of the capsule shell, facilitating the release of corrosion inhibitors.

### 2.3 Mechanism of ion-responsive inhibitor systems

Besides the *in situ* photoaquation reaction of hexacyanocobaltate(III), ions in the corrosion system can also be used to change the state of the microcapsule. In general, the ions doped into the shell of the microcapsule may interact with the ions in the surrounding environment to form a precipitate. Such interaction results in structural disruption of the capsule shell, leading to the subsequent release of the encapsulated inhibitor (Fig. 3).

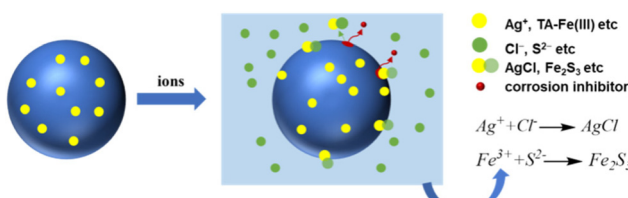


Fig. 3 Typical types of ion-responsive corrosion inhibitor system.

Ion-exchange between the ions in the shell and the corrosive ions in the external environment can also be used to release the encapsulated corrosion inhibitors in the microcapsule. Such ion exchange processes markedly diminish the corrosion rate of metals. Depending on the electronegativity of stimulus-responsive ions, ion-exchange inhibitor systems can be categorized into cationic and anionic types. Currently, most cationic exchange inhibitor systems use layered silicates (such as zeolite, montmorillonite, and kaolinite) as carriers. Owing to the isomorphous substitution of  $\text{Si}^{4+}$  and  $\text{Al}^{3+}$  in silicates, the negative charge in the framework is insufficient, facilitating the exchange of cations within the framework with environmental cations. Furthermore, organic ion exchange resin, ferricyanide, and zirconium orthophosphate are also candidates for shell materials in cation exchange inhibitor systems. Layered double hydroxides (LDH), such as hydrotalcite,<sup>61-66</sup> are among the most popular anion exchange inhibitor systems. LDHs have been investigated as storage media for functional anions,<sup>63,67-70</sup> including anionic corrosion inhibitors such as chromate,<sup>71,72</sup> vanadate,<sup>61</sup> molybdate,<sup>73</sup> quinate,<sup>74</sup> 2-mercaptopbenzothiazolate,<sup>74</sup> tungstate,<sup>75-77</sup> and other organic anions. Chloride in the corrosion medium can efficiently initiate the release of these inhibitory anions, which can subsequently be used as corrosion inhibitors for metals.

### 2.4 Other types of smart inhibitor system

Besides the aforementioned smart inhibitor systems, magneto-responsive, temperature-responsive, and redox-responsive inhibitor systems have also been developed.

Magneto-responsive microcapsules primarily consist of a capsule shell containing magnetic particles, including iron oxides such as magnetic ( $\text{Fe}_3\text{O}_4$ ) and magnetite ( $\gamma\text{-Fe}_2\text{O}_3$ ), as well as pure metals (such as Fe, Co, and Ni), alloys (such as  $\text{CoPt}_3$  and  $\text{FePt}$ ) and spinel-type ferromagnets (such as  $\text{NiFe}_2\text{O}_4$ ,  $\text{MgFe}_2\text{O}_4$ , and  $\text{CoFe}_2\text{O}_4$ ). The permeability of the capsule shell can be altered under a magnetic field, facilitating the release of the corrosion inhibitor. Furthermore, the magnetic field provides control over the migration of the microcapsule in the corrosion medium or coating, enabling targeted release.<sup>78</sup>

Microcapsules with intrinsic temperature-responsive units can be used as smart inhibitor systems. For instance, poly(*N*-isopropyl acrylamide) (PNIPAm) exhibits typical lower critical solution temperature (LCST) behaviour. At low temperatures, the interaction between PNIPAm and water predominantly involves hydrogen bonding, which results in a solvated layer around the macromolecular chain and causes the macromolecule to adopt a stretched nematic structure. As the temperature increases, there is a sudden shift in the interaction parameters between PNIPAm and water, leading to the disruption of some hydrogen bonds. Consequently, the solvation layer in the hydrophobic region of the macromolecular chain is destroyed, prompting the macromolecule to transition from a loose nematic structure to a compact gelatinous granular structure. Such a temperature-respon-



sive aggregated structure can also be used in smart inhibitor systems.

With regard to electrochemical corrosion, one of the most suitable stimuli is electrochemical redox, owing to its merits such as *in situ* generation, uniform distribution, robust reduction, and consistent decrease during corrosion. In comparison with barrier-type polymers, intrinsically conductive polymers (ICPs), such as polypyrrole (PPy) and polyaniline (PANI), possess inherent oxidation capabilities. Disulfide bonds are relatively stable under mild oxidation conditions but can be readily broken under reductive conditions. Consequently, employing these substances to design and construct smart corrosion inhibitors presents a highly suitable approach to directly respond to the electrochemical corrosion process.<sup>74,79</sup>

### 3 Different types of smart corrosion inhibition system and their applications

#### 3.1 Design and application of pH-responsive inhibitor systems

The alteration in pH serves as one of the most effective triggers for smart corrosion inhibitors. These inhibitors can respond to local acid–base fluctuations within the microanode/cathode region by releasing corrosion inhibitors, thereby halting the progression of corrosion. Smart corrosion inhibitors are often integrated with coatings to create complex anti-corrosive layers. Depending on the pH range of the reaction, these smart inhibitors can be categorized as acidic-sensitive, alkaline-sensitive, and mixed-sensitive. Furthermore, based on the assembly method, they can be classified into the following types: polyelectrolyte type, doped pH-sensitive component type, valve type, and grafting *via* covalent bond type.

As shown in Fig. 4, acid-sensitive polyelectrolytes, such as Eudragit E100, begin to dissolve when the pH is below 5 and the dissolution rate increases as the acidity increases.<sup>80</sup> PSS-PAH polyelectrolyte is usually used as a capsule wall because macromolecules can penetrate the capsule at low pH (<6),

while they are excluded at high pH (>8), and this transition is reversible. The integration of carbon hollow spheres, melamine, formaldehyde, and PTT is a common structure for developing smart corrosion inhibitors. This is based on the observation that ester groups hydrolyze more effectively in alkaline conditions. Therefore, these microcapsules exhibit higher corrosion inhibitor release rates in alkaline environments.<sup>81–84</sup>

The introduction of corrosion inhibitors such as cerium nitrate or 8-hydroxyquinoline (8-HQ) into microcapsules can provide a self-healing function. 8-HQ is released to form complexes with magnesium ions, which can precipitate and block the corrosion site. Under ultraviolet light,  $Mg(8-HQ)_2$  also exhibits fluorescent characteristics in scratched areas.<sup>83</sup> Certain polyelectrolyte microcapsules demonstrate responsive release under both acidic and alkaline conditions. This phenomenon is attributed to the increased concentration of cations or anions as the pH value decreases or increases, respectively. The additional positive or negative charge preferentially adsorbs to the negatively or positively charged polyelectrolytes, disrupting the electrostatic interaction balance between polyelectrolytes with opposite charges. This increase in electrostatic repulsion between the polyelectrolyte chains elongates their mutual distance, leading to the swelling of the shell. For instance, a corrosion inhibitor microcapsule composed of DDAC/SPSS/(BTA/SPSS)<sub>2</sub>/PDDAC/SPSS maintains stability in near-neutral pH environments (5–9). In this instance, the electrostatic forces between BTA, SPSS, and PDDAC, which have opposite charges, reach equilibrium. This results in a contracted state of the multilayer film while storing the BTA inhibitor within the shell. However, when the solution pH is either below 2 or above 11, the polyelectrolyte membrane expands and BTA is released, achieving corrosion inhibition rates of 64% and 71%, respectively.<sup>85</sup>

Deprotonation of polyelectrolytes serves as an alternative method to achieve pH responsiveness. The microcapsules are composed of poly(acrylic acid) (PAA) and polymethacrylic acid (PMA), which dissolve at a pH above 11.5 or below 2.5, respectively (Fig. 5). As the pH decreases, the carboxyl groups of PMA progressively become protonated, leaving only a minimal number of ionic pairs between PAH and PMA. This process results in an uncompensated ammonium group within the polycyclic aromatic hydrocarbon. The electrostatic repulsion



Fig. 4 Schematic illustration of the pH-responsive inhibitor system with Eudragit E100. Reproduced with permission<sup>80</sup> from Elsevier.

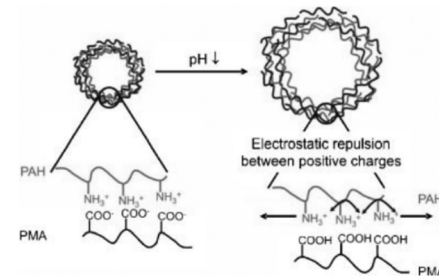


Fig. 5 Swelling model of (PAH/PMA)<sub>2</sub> capsules under acidic conditions. Reproduced with permission<sup>86</sup> from Wiley.



between the positive charges causes the entire structure to swell. Furthermore, the attraction of the polycyclic aromatic hydrocarbon for counterions can increase the local osmotic pressure, thereby enhancing the swelling effect.<sup>86</sup>

The application of polyelectrolytes, in conjunction with coatings, can facilitate the self-healing of these coatings. For instance, when the PEI/PSS + 8-HQ smart microcapsule structure is incorporated into a coating, no anodic activity or corrosion products are detected upon the emergence of local defects on the coating surface. This suggests that the release of 8-HQ serves to protect the substrate.<sup>87</sup> Nanocontainers with a  $\text{SiO}_2/\text{PEI}/\text{PSS}/\text{BTA}/\text{PSS}/\text{BTA}$  layered structure were used in combination with zirconium silicate-based hybrid films as anticorrosive coatings.<sup>88</sup> The formation of  $\text{SiO}_2\text{-Al}$  bonds between the silica and the substrate improved the adhesion between the coating and the metal substrate. Artificial defects were introduced into the coating, and after 24 hours of immersion, significant cathodic activity was observed at the induced defects for undoped  $\text{ZrO}_x/\text{SiO}_x$  thin film coatings. The activity increased with increasing immersion time. In contrast, doped  $\text{ZrO}_x/\text{SiO}_x$  film coatings exhibited significant cathodic activity only after 24 hours but repassivated again after 2 hours and remained healed after 48 hours. The corrosion inhibitor imidazole was encapsulated in halloysite nanotubes (HNTs) using vacuum sealing technology. Another inhibitor, dodecylamine, was added to a multilayer polyelectrolyte consisting of polyethylenimine and sulfonated polyetherketone, and HNTs were formed using the LbL technique. These HNTs (3 wt%) were fully dispersed in an epoxy resin matrix to form a smart hybrid self-healing polymeric coating. In comparison with the control coating, the modified coating and the hybrid coating showed corrosion inhibition efficiencies of 92% and 99.8%, respectively.<sup>26</sup>

Silk fibroin ionic microcapsules were successfully synthesized using the method of ion pairing and covalent cross-linking. These microcapsules demonstrated significant, highly reversible pH-responsive behavior, with a maximum volume swelling ratio of 800% under conditions where the pH was either lower than 2.0 or higher than 11.0. When the pH value decreased below 2.5, the zeta potential increased to positive due to the carboxylic groups on SF-PG being protonated below their  $\text{p}K_a$ . Conversely, when the pH exceeded 9, the zeta potential of the microcapsule became excessively negative due to the amino groups on SF-PL being deprotonated. Moreover, these silk fibroin ionic microcapsules exhibit pH-triggered permeability, thereby facilitating pH-controlled encapsulation and release.<sup>48</sup> By integrating ester groups and disulfide bonds, acid-base-sensitive smart responsive microcapsules can be designed and prepared, which hydrolyze into a shell matrix under both alkaline and acidic conditions.<sup>89</sup> Lignin was utilized to construct a smart responsive corrosion inhibitor, LMS@BTA. Under alkaline conditions, the deprotonation of BTA accelerated the dissolution and solubilization of lignin and disrupted the hydrogen bonds between lignin and BTA, resulting in rapid BTA release. Interestingly, although BTA is a neutral molecule, under acidic conditions, BTA becomes proto-

nated cations carrying a large number of positive charges, causing BTA molecules to repel each other and be released from LMS@BTA. Additionally, the concentration difference of BTA inside and outside the microspheres facilitates rapid release followed by slow release.

By creating artificial scratches on the surfaces of the WEP coating and the LMS@BTA/WEP coating, the self-repairing properties of the coatings are tested. After soaking for 48 hours, the  $Z_{0.01\text{Hz}}$  value of LMS@BTA/WEP is six times that of the WEP coating, indicating that it possesses good anti-corrosion and self-healing properties.<sup>90</sup> Resin, primarily composed of resorcinol, exhibits alkaline sensitivity. By utilizing this resin as a wall material and  $\text{NaNO}_2$  as an inhibitor, pH-sensitive microcapsules can be prepared. When the pH exceeds the  $\text{p}K_a$  value of 7.2 for the resin acid, it facilitates the dissociation of the resin acid in its deprotonated state. At an elevated pH of 12.6 and 9.1, there is a greater release of the microcapsules, with a rate of 44% over a span of 350 hours. As shown in Fig. 6, the  $\text{OH}^-$  present in the solution bind to and dissolve portions of the shell layer, thereby increasing the porosity of the microcapsules and enhancing the diffusion of the encapsulated substances.<sup>91</sup>

The nanovalve-type smart corrosion inhibitor system is usually composed of an encapsulating substance, a corrosion inhibitor, and a carrier. The carrier's role is to load the corrosion inhibitor, typically nanotubes or mesoporous materials, while the encapsulating substance seals the carrier to prevent leakage of the corrosion inhibitor. When the pH changes, the encapsulating substance dissolves, releasing the corrosion inhibitor, for instance, by integrating 8-HQ corrosion inhibitor into halloysite nanotubes, encapsulating Cu-8-HQ coordi-

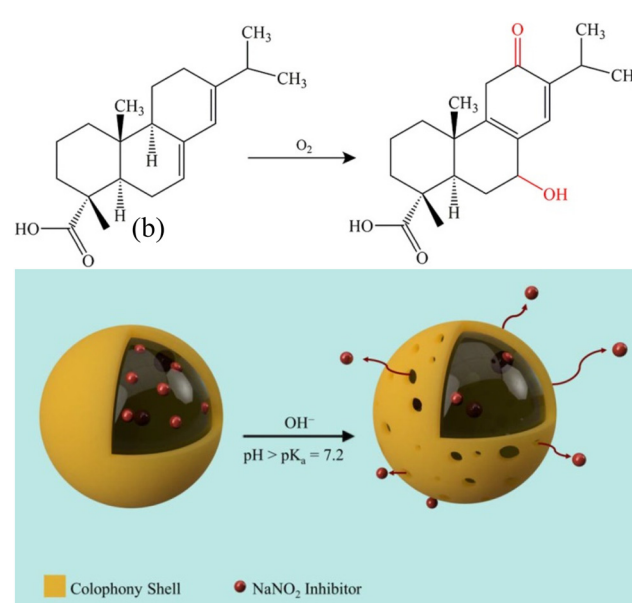


Fig. 6 Chemical structure of rosinic acid oxidation in solution and schematic illustration of the controlled release mechanism of resin microcapsules containing  $\text{NaNO}_2$  inhibitor via  $\text{OH}^-$ -induced porosity of the microcapsules. Reproduced with permission<sup>91</sup> from ACS.



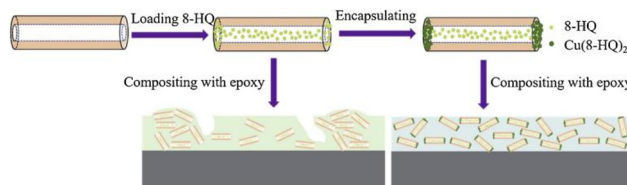


Fig. 7 Schematic illustration of the preparation of Cu-8-HQ@HNTs and Cu-8HQ@HNTs/epoxy coatings. Reproduced with permission<sup>92</sup> from Elsevier.

nation fillers, and subsequently blending Cu-8-HQ@HNTs with epoxy resin to create a Cu-8-HQ@HNTs/epoxy coating (Fig. 7). At a pH of 3, the cumulative release amount of 8-HQ in Cu-8-HQ@HNTs is approximately 80%. The self-healing ability of the Cu-8-HQ@HNTs/epoxy coating is due to the dissolution of the carbon nanotube end plugs, triggered by acidification in the coating edge area, which is followed by the release of 8-HQ from the carbon nanotubes.<sup>92</sup> Cu-BTA-Na<sub>2</sub>MoO<sub>4</sub>-HNTs<sup>93</sup> and Cu-BTA-MBT-HNTs can also be prepared in accordance with this principle.<sup>94</sup>

A similar structure was achieved by using hollow mesoporous silica spheres (HMSs) as carriers, with benzotriazole (BTA) incorporated as a corrosion inhibitor. As shown in Fig. 8, the HMSs surface was modified with 3-chloropropyl-triethoxysilane and 1,4-butanediamine, which can form a host-guest system with CB[6] macrocycles on the HMSs' surface, resulting in capped functionalized HMSs. In a neutral solution, the 1,4-butanediamine units of the stems exist in a protonated form, allowing them to form highly stable inclusion complexes with CB[6]. The deprotonation degree of the amino group from the stems significantly influenced the initial release rate. The maximum release rate of microcapsules was observed at the most alkaline condition, due to the enhanced extraction of hydrogen ions in alkaline solutions.<sup>95</sup>

The integration of corrosion inhibitors with carriers featuring unique bonds constitutes another method for creating smart corrosion inhibitors. These special bonds are designed to disintegrate under environmental stimuli, triggering the release of the corrosion inhibitor. Mesoporous or layered structures serve as optimal carriers for these inhibitors. Besides mesoporous silica and ceria, other carrier materials such as MOF, graphene-like structured MXenes, hydroxyapatite, and halloysite nanotubes have also been extensively studied.

The release of certain smart corrosion inhibitors is governed by the principle of electrostatic repulsion.<sup>18,96-98</sup> Hollow mesoporous zirconium dioxide was synthesized using MBT corrosion inhibitor and silica nanoparticles as a template. Under acidic conditions, both the zirconium dioxide particles and the MBT surfaces possess positive charges. Conversely, they exhibit negative charges under alkaline conditions.<sup>98</sup> Nanotube hybrid responsive microcapsules, such as the smart inhibitor nanocontainer, were fabricated using halloysite nanotubes and reduced graphene oxide (rGO). Subsequently, L-histidine (L-His) was adsorbed onto HNTs-rGO via electro-

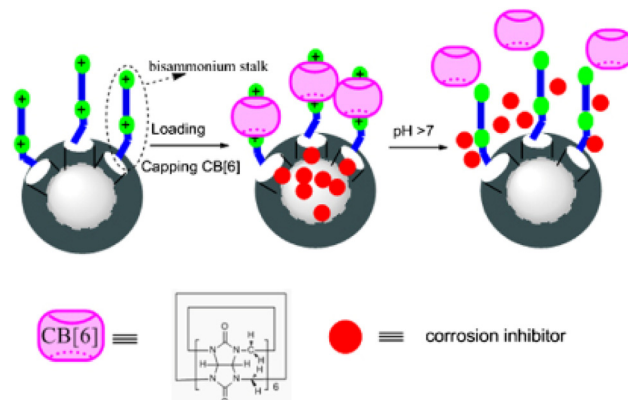


Fig. 8 Schematic illustration of the nanovalve-type smart responsive corrosion inhibitor with CB[6] macrocycle. Reproduced with permission<sup>95</sup> from IOP.

static adsorption, resulting in a ternary nanocomposite material with pH-responsive properties. L-His and HNTs-rGO carried positive charges within the pH range of 1.82 to 5.5. However, between pH values of 7.59 and 9.17, they both carried negative charges, leading to mutual repulsion. Within the pH range of 5.5 to 7.59, L-His and HNTs-rGO had opposite charges and attracted each other. Consequently, in the release test, even at pH 9, 90.0% of the adsorbed L-His was released. This structure has the potential to extend the lifespan of coatings.<sup>99</sup> The incorporation of Fe<sup>3+</sup> (FeCl<sub>3</sub>) into functionalized mesoporous silica activates the cation during the adsorption of corrosion inhibitor ions. Under alkaline conditions, the mesoporous silica post-adsorption of the corrosion inhibitor (MSInh) becomes negatively charged, which facilitates electrostatic repulsion between MSInh and molybdate ions. This results in a more rapid release of these ions under such conditions. Conversely, in acidic environments, manganate and molybdate possess opposing charges. Consequently, their mutual attraction leads to a decreased release of molybdate from MSInh. Therefore, employing MSInh nanocontainers in near-neutral and alkaline media is an effective strategy for enhancing the release of MSInh in corrosive environments (Fig. 9).<sup>18</sup> A novel graphene structure based on carbon hollow spheres (CHSs) was also used as microcapsules.<sup>100</sup>

MOF structures can release bound corrosion inhibitors in an acidic environment. This is due to the binding of protons, acting as Lewis acids, to the oxygen atoms of the MOF. This interaction disrupts the linkage between the carboxylic group and the metal center of the MOF, leading to the release of BTA. Furthermore, the stable protonated form of the corrosion inhibitor BTA (BTAH<sup>2+</sup>) in an acidic solution also disrupts the bond between the BTA carboxylic group and the MOF.<sup>101,102</sup>

When such a structural corrosion inhibitor is used in conjunction with organic tannic acid (TA) and inorganic praseodymium (Pr), an ion exchange process is triggered. This process releases the trapped inhibitor from ZIF8 due to the corrosive action of Na<sup>+</sup>, Cl<sup>-</sup>, H<sup>+</sup>, and OH<sup>-</sup>. At high pH conditions, Pr<sup>3+</sup> and Zn<sup>2+</sup> react with OH<sup>-</sup> to generate a protective hydroxide



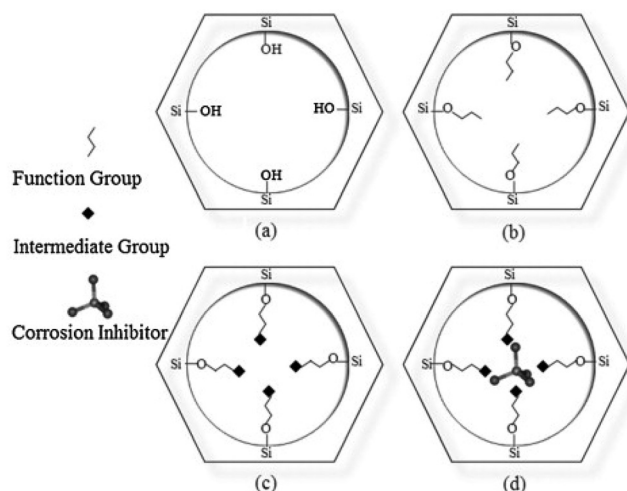


**Fig. 9** Schematic illustration for (a) cylindrical mesoporous silica, (b) mesoporous silica functionalization, (c) FeCl<sub>3</sub> compound adsorption, and (d) the corrosion inhibitor adsorption process. Reproduced with permission<sup>18</sup> from Elsevier.

layer at the cathodic zone. Conversely, at low pH conditions, the formation of Pr-tannic acid-Fe, Zn-tannic acid-Fe, and/or Pr-MI-Fe complexes in a ferrous medium can lead to the formation of an inhibition film at the anodic region.<sup>103</sup>

MXenes, a type of smart responsive corrosion inhibitor, are exemplified by the Ti<sub>3</sub>AlC<sub>2</sub> substrate with interlayer Ti<sub>3</sub>C<sub>2</sub> MXene sheets formed through HF etching. These thin sheets were subsequently modified with 3-aminopropyltriethoxysilane (APTES) to graft -NH<sub>2</sub> groups and coated with cerium ions (Ce<sup>3+</sup>), serving as an eco-friendly corrosion inhibitor. This was accomplished by utilizing the superior adsorption and intercalation ability of Ti<sub>3</sub>C<sub>2</sub>T<sub>x</sub> for cations (Fig. 10). The increased release under acidic conditions is ascribed to the protonation of surface functional groups (-NH<sub>2</sub>, -F, -O, and -OH) of MXene. EIS results showed that after 24 hours of exposure to a normal saline solution, |Z|<sub>0.01Hz</sub> was approximately 8.9 kΩ cm<sup>2</sup> for the epoxy resin coating and approximately 32.1 kΩ cm<sup>2</sup> for

the MXene-Ce<sup>3+</sup>@EP coating, indicating a significant improvement in the corrosion resistance of the coatings.<sup>49,50</sup>

Hydroxyapatite (HAP) can be used as a reservoir for various inhibitors, including Ce(III), La(III), salicylaldoxime (Sal), and 8-hydroxyquinoline. Inorganic cations, particularly Ce<sup>3+</sup> and La<sup>3+</sup>, can permeate HAP via an ion exchange mechanism. Organic inhibitors such as Sal and 8-HQ may be adsorbed, while 8-HQ forms a stable complex with Ca<sup>2+</sup>. The dissolution of HAP by inorganic inhibitors commences at pH values below 6 and is further accelerated at pH below 3.1. However, this strategy does not apply to organic inhibitors (Sal and 8-HQ). Their release begins at microalkaline levels and concludes at pH 2, when HAP is completely dissolved.<sup>104</sup>

Utilizing the reversibility of Schiff base bonds, recyclable smart corrosion inhibitors were developed. Three representatives, namely the amino acids glycine, alanine, and leucine, were immobilized onto microspheres via the Schiff base reaction. In an acidic environment, glycine was almost entirely released. Subsequent to the release of these amino acids, formaldehyde groups were regenerated, facilitating the recycling of the microspheres. These recycled microspheres exhibited a corrosion inhibition rate of 74.7%.<sup>105</sup> By employing an acid-labile β-thiopropionic acid bond, polymerizable derivatives of 8-HQ were synthesized under acidic conditions (pH = 3.5). Notably, these polymer nanoparticles released over 95% of the 8-HQ within a time range of 14 days. Conversely, under neutral conditions (pH = 7.0), the release rate was markedly slower, achieving only 15% in the same time range.<sup>51</sup>

### 3.2 Design and application of photoresponsive inhibitor systems

Gold nanoparticles predominantly absorb visible light around 520 nm, while the primary absorption region of silver nanoparticles spans the wavelength range of 380–430 nm. The location of maximum absorption is significantly influenced by particle size and shape.<sup>106,107</sup> Upon photoabsorption, nanoparticles generate heat, which subsequently destroys the capsule wall and releases the encapsulated substance. Skirtach *et al.* pioneered the use of noble metal nanoparticles for optically induced changes in microcapsule shells by integrating silver nanoparticles into PAH/PSS microshells to examine their photoresponsive behavior.<sup>53</sup> In recent years, there has been a significant increase in research on doping metal oxide nanoparticles (such as TiO<sub>2</sub>, ZnO, Fe<sub>2</sub>O<sub>3</sub>, Fe<sub>3</sub>O<sub>4</sub>) and noble metal nanoparticles (such as AgNPs, AuNPs) onto two-dimensional and three-dimensional LbL multilayer structures.<sup>108,109</sup> These photosensitive microcapsule structures are often cored with materials like CaCO<sub>3</sub>,<sup>110,111</sup> and the capsule walls can be composed of polyelectrolytes, liposomes,<sup>112</sup> or hydrogels.<sup>113</sup>

Microcapsules of polyelectrolyte structures, such as the (PDADMAC/Au/PSS)<sub>4</sub> microcapsule structure, can achieve reversibility. This is achieved by increasing the temperature slightly above the glass transition temperature ( $T_g$ ) of the polyelectrolyte complex. At elevated temperature, NPs absorb the generated heat, causing the polymer network surrounding the NPs to melt locally, thereby increasing the permeability of the

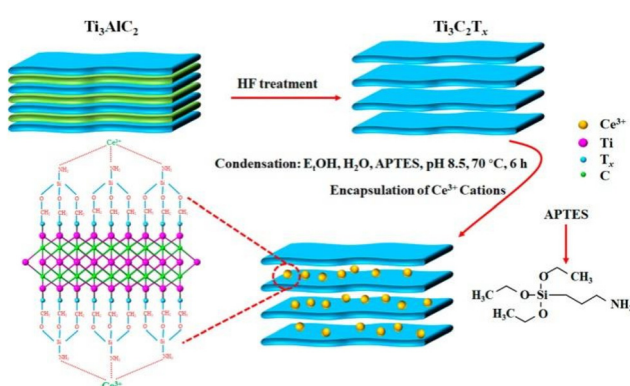


**Fig. 10** Schematic illustration of the preparation, surface modification, encapsulation principle and inhibition mechanism of Ti<sub>3</sub>C<sub>2</sub> MXene-Ce<sup>3+</sup> coating. Reproduced with permission<sup>50</sup> from ACS.



membrane. When the laser is turned off, the melted polyelectrolytes cool below  $T_g$ , prompting the nanofilm to self-seal. Under a laser power of 60 mW, 100% of the capsules were found to open.<sup>55</sup> Gold nanoparticles do not inherently absorb near-infrared (NIR) light. However, they can be aggregated into larger structures by adding salt ions or other chemicals, resulting in an NIR absorption band. For instance, AuNP aggregates are synthesized using a NaCl solution and hollow shells are constructed with citrate and functionalized polyelectrolytes PDADMAC and PSS. These polyelectrolytes can be functionalized in both homogeneous (non-aggregated) and aggregated (one peak in the NIR spectrum) states. Capsules containing gold particle aggregates exhibit a release of encapsulated materials under low-power NIR laser irradiation, while those without gold particle aggregates show no release at all.<sup>108</sup> Laser and pH dual-responsive micro/nano-reservoirs can also be prepared by doping noble metal particles into the polyelectrolyte shell. Compared with pH-stimulated release, laser-stimulated release of corrosion inhibitors is three times faster, which can effectively give better anti-corrosion performance.<sup>36</sup>

The photoresponsive mechanism of titanium dioxide differs from that of metal nanoparticles, utilizing photocatalytic properties.<sup>52</sup> As shown in Fig. 11, polyelectrolyte doped with  $\text{TiO}_2$  is employed to encapsulate the corrosion inhibitor by forming microcapsules. Upon exposure to ultraviolet light, the  $\text{TiO}_2$  within the microcapsule becomes excited, generating electron–hole pairs. The holes situated at the valence band of  $\text{TiO}_2$  exhibit pronounced oxidative activity. Functional groups such as  $-\text{NH}$  and  $-\text{SO}_3^-$ , PSS, and PEI are highly sensitive to variations in the density of the surrounding electrons (or ions). Any alteration in the chemical state of these functional groups can disrupt this relatively weak interaction, ultimately leading to the release of the corrosion inhibitor. Mesoporous  $\text{TiO}_2$  loaded with BTA is encapsulated by PEI and PSS to form a photoresponsive microcapsule. When this microcapsule is integrated with the coating, it significantly repairs coating defects under ultraviolet light irradiation, and the encapsulated corrosion inhibitor markedly reduces the corrosion process.<sup>36</sup> Similar structures have been tested electrochemically, demonstrating that after UV irradiation, the Nyquist diagram successfully reverted to its original shape. The corrosion inhibitor played a supportive role, while a pure  $\text{TiO}_2$  NPs coating could not restore the cor-

roded surface to its original state.<sup>114</sup> Polyelectrolytes with aromatic groups can also be constructed into photoresponsive microcapsules. It has been found that capsules composed of polyelectrolytes containing aromatic groups, such as PSS, undergo significant shrinkage under ultraviolet light irradiation. For instance, upon exposure to  $20 \text{ mW cm}^{-2}$  for 60 minutes, the size of five double-layer PDDA/PSS capsules decreased by approximately 80%. Ultraviolet light irradiation triggers chemical changes in aromatic polyelectrolytes, evidenced by the disappearance of aromatic bands and the generation of by-products such as  $\text{SO}_4^{2-}$ . These ultraviolet-induced changes in the chemical composition of capsules lead to structural reconstruction and shrinkage.<sup>58</sup>

In addition to noble metal particles, infrared dyes and porphyrins can also induce photoabsorption. Silver nanoparticles or an infrared dye were integrated into the polyelectrolyte shell of PAH/PSS capsules. For those doped with an infrared dye, where the dye is only adsorbed on the outer layer, a higher intensity was necessary to activate these capsules using a laser compared with those containing silver nanoparticles. The observed effect for Ag nanoparticle-doped capsules was due to the direct local heating of the nanoparticles, whereas IR-806 dye-doped capsules ruptured due to heating induced by electron–vibration–phonon energy conversion.<sup>53</sup>

Photosensitive microcapsules can be constructed from photoisomerizable or photo-oxidized substances. Azobenzene (azo), a class of molecules that react to both near-ultraviolet and visible light, is composed of two phenyl groups linked by an  $\text{N}=\text{N}$  double bond. The ultraviolet absorption reaction of azobenzene occurs through a reversible internal rearrangement known as *cis*–*trans* isomerization. This isomerization process is typically reversible. Recent studies have demonstrated that lipid vesicles containing azo groups can germinate into multiple vesicles under ultraviolet light and fuse with each other under green light. Diazo resin (DZR) forms covalent bonds with polyacrylic acid or PSS in LbL films under ultraviolet light. Similarly, the composite shell of DZR and PSS can also polymerize under ultraviolet light. The resulting cross-linked DZR/PSS microcapsules exhibit superior mechanical stability compared with those not exposed to light. Taking advantage of this property, photoresponsive microcapsules with a structure of  $(\text{PAH/PAZO})_3\text{PAH/PVS}$  were prepared. After 10 hours of light exposure, their diameter decreased to approximately 45% of the original size.<sup>57,110</sup>

Photoresponsive microcapsules can also be fabricated using the salt-sensitive star polyelectrolyte. The  $\text{K}_3[\text{Co}(\text{CN})_6]$  salt possesses the capability to decompose into monovalent and divalent ions when subjected to UV light irradiation (eqn (1)).  $(\text{PSS/PMETAI18})_n$  photosensitive microcapsules were synthesized for which permeability can be adjustable. Introducing a minor quantity of  $\text{K}_3[\text{Co}(\text{CN})_6]$  salt markedly diminished the permeability of the  $(\text{PSS/PMETAI18})_n$  shell, leading to a notable reduction in pore size. The presence of trivalent hexacyanocobaltate(III) ions induced the collapse of the PMETAI star polyelectrolyte at low concentrations, potentially due to the combined effects of arm chain collapse and inter-star

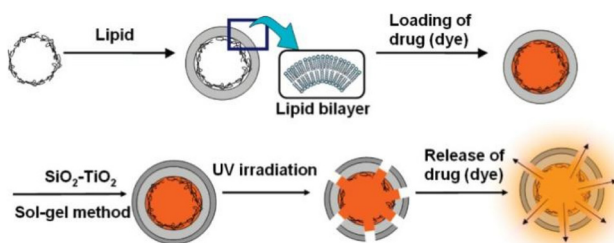
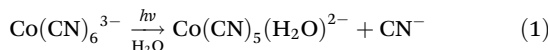


Fig. 11 Preparation procedure of drug (dye) controlled release UV-responsive  $(\text{PSS/PDDA})_5/\text{PSS/DDAB}/\text{SiO}_2\text{--TiO}_2$  capsules. Reproduced with permission<sup>52</sup> from ACS.



attraction between PMETAI18 stars. Subsequently, the decomposition of  $K_3[Co(CN)_6]$  salt into monovalent and divalent ions under UV light restored the permeability and size of the  $(PSS/PMETAI18)_n$  microcapsules. This photoinduced alteration in microcapsule permeability is entirely reversible.<sup>59</sup>



### 3.3 Design and application of ion-responsive inhibitor systems

**3.3.1 Precipitation type.** Ions play a significant role in influencing electrochemical reactions. An increase in ion concentration enhances the conductivity of the solution, thereby promoting corrosion activity. Chloride has the propensity to damage the film layer, facilitating localized corrosion due to its small radius. On the other hand, sulfide ions ( $S^{2-}$ ) readily combine with iron ions to form iron sulfide. This compound is not only flammable and explosive, creating a hazardous source, but it is also not dense and leads to localized corrosion on metal surfaces. Some researchers have explored the use of these ions as trigger sources for smart microcapsules. By selecting silver ions ( $Ag^+$ ) and alginate for the formation of capsule wall materials, and utilizing the precipitation reaction between  $Ag^+$  and  $Cl^-$ , the capsule can be decomposed when in contact with chloride ions, thereby releasing the substances inside. A similar metal ion is lead ions ( $Pb^{2+}$ ).<sup>115</sup> A novel metal-phenolic supramolecular membrane, TCS@CTAB-(TA-FeIII)<sub>20</sub>, is responsive to sulfide ions. The release of TCS was triggered by an increase in sodium sulfide concentration above 10 mM. The release of TCS was caused by the disintegration of the metal-phenolic membrane due to the ability of the  $S^{2-}$  anion to trap  $Fe^{3+}$  ions from TA-FeIII, forming a stable  $Fe_2S_3$  substance.<sup>116</sup>

**3.3.2 Ion exchange type.** Ion exchange models can be categorized into cationic and anionic types, depending on the specific substances they are designed to load.

Cationic type predominantly exchange with  $Na^+$  and  $K^+$ . For instance, in the  $Zn_2Fe(CN)_6$  structure,  $Zn^{2+}$  is replaced by  $K^+$  and  $Na^+$  in solution. As shown in eqn (2), the  $Zn^{2+}$  liberated from  $Zn_2Fe(CN)_6$  forms a protective layer on the cathode, thereby mitigating localized corrosion.<sup>117,118</sup> After two weeks of immersion, the impedance of the coating containing  $Zn_2Fe(CN)_6$  remained largely unchanged, indicating superior anticorrosion performance. In contrast, the impedance of the coating devoid of  $Zn_2Fe(CN)_6$  decreased by 50 times.<sup>37</sup> Numerous researchers have successfully modified montmorillonite to construct Ce(III)-MMT ion-responsive structures. At shorter immersion durations (1 h), the low-frequency impedance increased by two orders of magnitude compared with unmodified silanes.<sup>119</sup> Similarly, sodium montmorillonite (Na-MMT) can serve as a nanocontainer (Fig. 12) to load  $Zn^{2+}$  and imidazole inhibitors, thereby enhancing the protective properties of epoxy resin coatings.<sup>120</sup> Natural bentonite clay minerals can also be employed as novel cation exchange carriers.<sup>121</sup>  $Ca^{2+}$  can function as exchange ions, as evidenced by

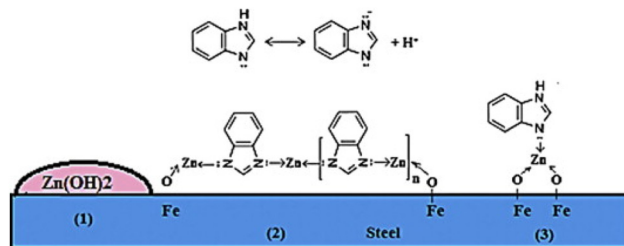
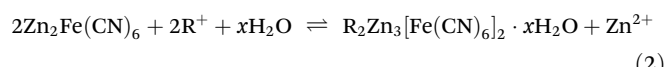


Fig. 12 Adsorption model of inhibitors released by Zn-MMT + BIA-MMT within artificial defects on steel surfaces. Reproduced with permission<sup>120</sup> from Elsevier.

their exchange with bituminous clay minerals. When the  $Ca^{2+}$ -BDT sample was immersed in a 0.1 M NaCl solution, nearly all of the  $Ca^{2+}$  was released after 15 h. Even after soaking in the same solution for 20 h,  $Ca^{2+}$  release persisted. After interacting with a 0.1 M NaCl solution for 20 h, the inhibition efficiency of  $Ca^{2+}$ -BDT reached 91%.<sup>122</sup>



The efficacy of bentonite pigments with exchangeable  $Zn^{2+}$  in inhibiting corrosion is markedly enhanced. In contrast, smart-release bentonite pigments containing exchangeable cerium(III) and yttrium(III) cations demonstrate negligible effectiveness in decelerating the propagation rate of filiform corrosion (FFC) induced by chloride.<sup>63</sup> Nonetheless, anion-exchanged hydrotalcite (HT)-based pigments emerge as potent inhibitors for FFC. In a NaCl solution, magnesium aluminum layered double hydroxide laden with tungstate anion,  $LDH-WO_4^{2-}$ , adsorbs corrosive chloride ions while simultaneously releasing interlayer corrosion inhibitor  $WO_4^{2-}$  anions, achieving an inhibition rate of up to 97%. A structurally analogous system features a reservoir composed of nanostructured Mg/Al and Zn/Al layered double hydroxides, with the interlayer region housing isocyanate anions. These nanocrystalline layered double hydroxides can regulate the release of vanadate ions, exhibiting commendable corrosion inhibition properties.<sup>65</sup> Furthermore, Zn/Al doped LDH nanocontainer (Fig. 13) coatings demonstrate notable self-healing capabilities.<sup>61,123</sup> Amphoteric exchangeable ions have also been extensively researched. For instance, it has been determined that amphoteric Zn-Al-[ $V_{10}O_{28}$ ]<sup>6-</sup> hydrotalcite ion exchange compounds can facilitate the exchange of vanadate with  $Cl^-$  and  $Zn^{2+}$  with  $Na^+$  when subjected to NaCl solutions ranging from 0.0001 M to 1.0 M.<sup>124</sup>

### 3.4 Design and application of magnetic-responsive inhibitor systems

Magnetic nanoparticles (NPs) hold potential for applications in magnetic fluids, catalysis, biotechnology/biomedicine, magnetic resonance imaging (MRI), data storage, and environmental remediation.<sup>78,125,126</sup> However, their intrinsic instability over extended periods and propensity to aggregate constrain



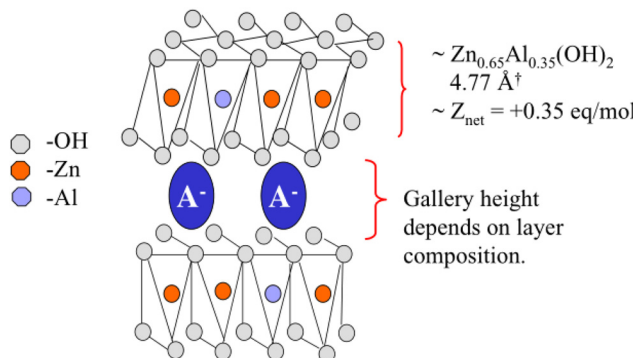


**Fig. 13** Schematic illustration of the layered structure of a hydroxalite compound. The structure consists of alternating layers of positively charged mixed metal hydroxide sheets and anions. Reproduced with permission<sup>61</sup> from Elsevier.

their utility. Coating the surface of magnetic NPs with polymers, silica, or other materials can prevent aggregation and facilitate functionalization. Among these coating materials, silica and carbon are particularly appealing due to their high biocompatibility and stability, low toxicity, and straightforward functionality.<sup>127</sup> The discovery of supramolecular self-assemblies of mesoporous materials has sparked significant interest across various research fields.<sup>127–130</sup> Magnetic mesoporous materials have been the focus of attention for integrating mesoporous structures with magnetic properties to achieve a magnetic response, high pore volume, large surface area, and ease of functionalization.<sup>38,131–139</sup> Magnetic nanocomposites with mesoporous structures can be removed after use by applying a magnetic field, or targeted delivery can be achieved using an external magnetic field. A new class of self-healing magnetic microcapsules was designed and synthesized from poly(urea formaldehyde) encapsulated in BTA and magnetic multi-wall carbon nanotubes (MWCNTs).<sup>38</sup> The magnetic targeted microcapsule coating (SMG) was prepared using the microcapsules. The magnetic microcapsules could migrate rapidly through the coating solution by applying a magnetic field. The SMG coating not only shortened the migration route of the released BTA, but also rapidly accelerated the formation of passivation film and hindered the corrosion of copper after mechanical damage of the coating. The corrosion inhibition rate of the magnetic self-healing coating could reach 91.2% within 4 h of immersion. Its self-healing efficiency was 6.4 times higher than that of the non-magnetic self-healing coating. Ferromagnetic gold-coated cobalt nanoparticles (Co@Au) embedded within the polyelectrolyte capsule wall can form magnetically sensitive microcapsules. (PSS/PAH)<sub>4</sub>(PSS/Co@Au)<sub>1</sub>(PSS/PAH)<sub>6</sub> microcapsules were 99% filled with FITC-dextran after 30 min of an alternating magnetic field, indicating that permeability of the microcapsules was caused by the low-frequency alternating magnetic field, allowing macromolecules normally excluded from the capsules to penetrate into the capsules. At frequencies less than 300 Hz, the lower the frequency, the faster the diffusion of FITC-dextran. The increase in frequency appeared to diminish the stirring effect

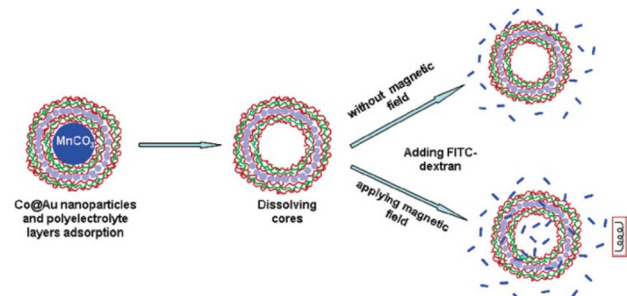


**Fig. 14** Scheme of Co@Au nanoparticle microcapsule assembly and magnetic permeability test under an oscillating magnetic field. Reproduced with permission<sup>131</sup> from ACS.

of the magnetic field on the Co@Au nanoparticles embedded in the capsule wall, thus reducing the permeability of the magnetic capsule<sup>131</sup> (Fig. 14). Magnetic fluids can also be composed of polyelectrolyte-stabilized magnetite nanoparticles. This new magnetic fluid has potential for *in vivo* MRI diagnostics.<sup>132</sup>

### 3.5 Design and application of temperature-responsive inhibitor systems

Smart nanocontainers can be engineered using stimulus-responsive polymers that exhibit temperature sensitivity. Capsules composed of the robust polyelectrolytes PDADMAC and PSS (with PDADMAC forming the first layer) display intriguing temperature-dependent behavior. Shells with an even number of layers, denoted as (PDADMAC/PSS)<sub>x</sub> where *x* ranges from 1 to 3, contract upon heating due to increasing wall thickness until they solidify into spheres. Conversely, shells with an odd number of layers, represented by (PDADMAC/PSS)<sub>x</sub>, expand up to five times their original size before rupturing above 55 °C. The swelling of PDADMAC/PSS microcapsules is attributed to the presence of a large number of positively charged monomers in PDADMAC end-sealed capsules. The inclination to reduce surface tension is counterbalanced by electrostatic forces, specifically repulsion between excess charges, resulting in swelling. In contrast, PSS end-sealed capsules maintain near charge balance. The primary force driving the contraction of charge-balanced capsules is the minimization of the water–polymer interfacial energy.<sup>133</sup> Silicon dioxide/polymer double-walled hybrid nanocapsules have been synthesized. Smart containers with controlled release capabilities are achieved by modulating the polymer shell. For instance, these nanocontainers can exhibit thermal responsiveness by incorporating poly(*N*-isopropylacrylamide-*co*-methylene bisacrylamide) shells. At 25 °C, PNIPAM shells tend to expand, while at 50 °C, they contract, effectively sealing BTA molecules within the lumen and inhibiting their diffusion out of the shell.<sup>134</sup>

### 3.6 Design and application of redox-responsive inhibitor systems

The most dependable stimulus is the alteration in electrochemical potential, as it is generated *in situ*, uniformly distrib-



uted and highly consistent with the actual situation. In contrast to barrier polymers, intrinsically conductive polymers, such as polypyrrole (PPy) and polyaniline (PANI), possess an inherent oxidizing capacity. Redox-sensitive PANI can be employed as a shell material to fabricate redox-responsive microencapsulated capsules.<sup>135</sup> The microcapsules were constructed with the corrosion inhibitor 3-nitrosalicylic acid (3-NiSA) as the core material and modified with gold nanoparticles to prevent direct contact between the metal and CP. When no potential was applied (simulating a complete coating), the polyaniline shell layer functioned as a gatekeeper to inhibit the release of the corrosion inhibitor from the core. The reduction of PANI (applying a low potential to simulate the onset of corrosion) resulted in an increase in the shell's permeability and the release of the inhibitor. Conversely, re-oxidation (application of a high potential to simulate metal passivation) led to a decrease in permeability and further release was prevented. Disulfide bonds are relatively stable under mildly oxidizing conditions but tend to break under reducing conditions. Microcapsules containing disulfide bonds were designed and developed. TBP was used as a reducing agent to break the disulfide bonds. The nanocapsules successfully released approximately 90% of the corrosion inhibitor MBT after 5 hours. In the absence of TBP triggering, no release of MBT was detected.<sup>79</sup> A sophisticated microcapsule, termed CP-SNCs, has been engineered to exhibit a responsiveness to corrosion potential stimuli and an expedited positioning capability.<sup>74</sup> This structure incorporates a supramolecular component, specifically a water-soluble bipyridine column aryl hydrocarbon, onto the external surface of a magnetic nanocarrier ( $\text{Fe}_3\text{O}_4@\text{mSiO}_2$ ), which is connected *via* a disulfide linkage. Upon application of the magnesium alloy's corrosion potential ( $-1.5$  V vs. SHE), 8-HQ is immediately released due to the disintegration of the disulfide linker and the removal of the supramolecular assemblies. These CP-SNCs were integrated into an organic-inorganic hybrid sol-gel coating to create corrosion potential-stimulated feedback anticorrosion coating (CP-SFAC), which was subsequently applied to the magnesium alloy AZ31B. In the presence of a magnetic field, the CP-SNCs aggregate near the AZ31B surface. The CP-SFAC demonstrates superior anti-corrosion properties and, notably, possesses a rapid self-healing function when localized corrosion occurs by a microzone electrochemical technique.

### 3.7 Design and application of multiple-responsive inhibitor systems

Smart response structures with dual or multiple responses are designed with the idea of assembling different response substances. For example, polyelectrolyte is combined with benzophenone (BP) moieties and gold nanoparticles to form a pH-light dual response. Polyelectrolyte is combined with disulfide bonds, polyaniline, polypyridine, HMON and other materials to form pH-redox double responsive system and so on. In addition, some substances exhibit dual responses simul-

taneously, such as Cu-BTA complex nanovalves that respond to both pH and  $\text{S}^{2-}$ .

**3.7.1 pH-photo-responsive inhibitor systems.** The structures of weak polyelectrolytes combined with UV-sensitive benzophenone (BP) moieties<sup>136</sup> and gold nanoparticles with polycyclic aromatic hydrocarbons (PAHs)<sup>111</sup> can be synthesized into pH-UV responsive and pH-IR responsive smart microcapsules. The charge density of AuNP, due to the presence of carboxyl groups on their surface, is pH-dependent. Consequently, these capsules possess the capability to deconstruct at both low and high pH levels.

**3.7.2 pH-redox responsive inhibitor systems.** By leveraging the pH sensitivity of polyelectrolytes and the redox sensitivity of materials such as disulfide bonds, polyaniline, polypyridine, and HMON, a dual-responsive smart microcapsule corrosion inhibitor can be synthesized. A ternary copolymer exhibiting both pH and redox responsiveness was synthesized by incorporating acetal and disulfide bonds into its structure. This design facilitates the selective release of two distinct corrosion inhibitors: benzoic acid and tryptamine. During the electrochemical corrosion process, proton generation on the anodic side prompts the hydrolysis of the acetal bonds, leading to the release of benzoic acid. Concurrently, the reduction of disulfide bonds results in the release of tryptamine. As shown in Fig. 15, the corrosion rate of steel coated with this dual-responsive ternary copolymer is diminished by a factor of 800 compared with uncoated steel.<sup>137</sup> A self-healing anticorrosive coating comprising a polyaniline-silica reservoir (PASR) was developed. Oxalic acid serves both as a corrosion inhibitor and dopant. Redox reactions at the metal/coating interface lead to the release of dopant ions from polyaniline, followed by metal passivation. If additional pores form in the coating, alkaline conditions induced by cathodic reactions on the metal surface will initiate corrosion within the PASR coating. Subsequently, when hydroxyl ions (produced by cathodic reactions) interact with the polyelectrolyte-covered silica reservoir, dopant ions are released.<sup>139</sup> PPy nanocapsules demonstrate dual pH and redox responsiveness.<sup>138,140,141</sup> At elevated pH levels, the degradation of polypyridine predominantly occurs due to nucleophilic attacks by  $\text{H}_2\text{O}$  and  $\text{OH}^-$ . This degradation compromises the integrity of PPy nanocapsules, resulting in the release of

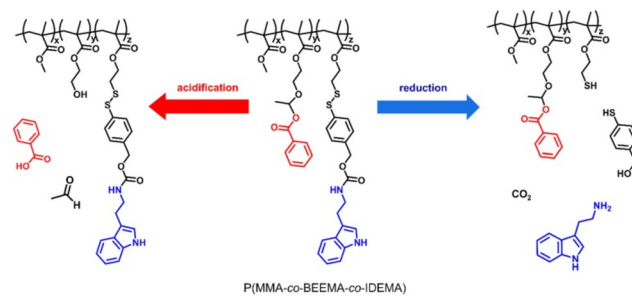


**Fig. 15** Selective release of the corrosion inhibitors benzoic acid (red) and tryptamine (blue) from a doubly reactive terpolymer by acidification and reduction. Reproduced with permission<sup>137</sup> from ACS.



corrosion inhibitors. As the pH decreases, anions neutralize the positive charge of protonated polypyridine structures, creating osmotic pressure that draws water molecules into the nanocapsules. Consequently, PPy nanocapsules expand, and their volumetric expansion facilitates the release of encapsulated corrosion inhibitors through surface openings or micro-cracks. This expansion also enhances the hydrophilicity of polypyridine nanocapsules, further promoting the release of encapsulated corrosion inhibitors. When a positive potential is applied, amine–amine intermolecular hydrogen bonding forms dense polymer chains that impede the release of loaded corrosion inhibitors. Conversely, a negative potential causes polypyridine nanocapsules to gradually decrease, weakening mineral–amine intermolecular hydrogen bonding and reducing the structural density of polypyridine nanocapsule shells.<sup>142,143</sup> After incorporating thioether groups into the shell, HMON materials exhibit unique drug-loaded responsive release under redox/acidic conditions.<sup>144</sup> A dual stimulus-responsive smart corrosion inhibitor system, MBT@HMON, was synthesized. Under the combined effects of redox and pH, the cumulative release amount of MBT reached 81.0%, and the inhibition rate was 81.31%.<sup>145</sup>

**3.7.3 pH-salt concentration responsive systems.** The capsules were fabricated by LbL adsorption of the oppositely charged polyelectrolytes, PSS and PAH, onto the surface of melamine formaldehyde and  $\text{CdCO}_3$  particles, followed by denucleation. The capsules remained closed at pH levels of 8 or higher, while macromolecules infiltrated their interior at pH levels below 6. Salt-induced rearrangement of polyelectrolytes results in localized defects, facilitating the penetration of small molecules such as fluorescein.<sup>146</sup> By utilizing mesoporous silica nanoparticles as carriers, the corrosion inhibitor BTA and biocide benzalkonium chloride were encapsulated within the mesopores to form Cu-BTA complex nano-valves at the openings. These valves exhibited release behavior when the pH was below 5 or when  $\text{S}^{2-}$  exceeded 0.02 mM (approximately 0.6 ppm). Under neutral water conditions (pH approximately 6.5–8), the BTA molecules remained encapsulated within the functionalized msn without premature release. At pH levels of 3 and 4, the release of loaded BTA reached 85% and 80% within 100 minutes, respectively. Spontaneous release occurred when the samples were immersed in higher concentrations (2 mM and 1 mM) of  $\text{Na}_2\text{S}$  solution. Even when the solvent was diluted 100-fold (to 0.02 mM), more than half of the release was observed.<sup>14</sup>

**3.7.4 pH-water responsive systems.** An innovative, eco-friendly active corrosion protection system for Aluminum Alloy 2024 (AA2024) has been developed. This system utilizes water-borne polyurethane coatings with 2-mercaptopbenzothiazole as a corrosion inhibitor and halloysite clay nanotubes as the carrier for this inhibitor. The LBL encapsulation of natural polyelectrolytes, specifically  $\epsilon$ -poly-L-lysine ( $\epsilon$ -PLL) and sodium alginate, was employed. Previous reports have indicated that the controlled release of MCs loaded with 2-MBT, typically containing a polyelectrolyte layer, is accompanied by water uptake. This leads to swelling, dissolution of 2-MBT, and outward

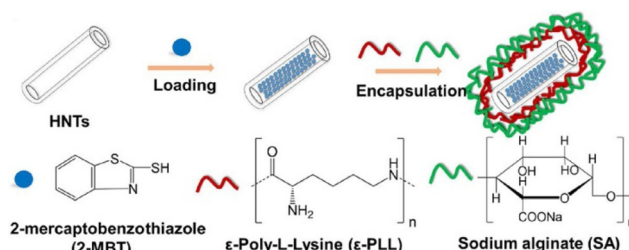


Fig. 16 Schematic illustration of the fabrication process of smart microcapsules (MCs). Reproduced with permission<sup>147</sup> from ACS.

diffusion of dissolved 2-MBT through the water-filled cavity into the external medium. The rate of water absorption is determined by the number of hydrophilic functional groups within the polyelectrolyte layer. Salt spray tests and electrochemical measurements have demonstrated that the scratch coatings embedded in MCs possess excellent self-healing properties. They form a released 2-MBT adsorption layer on the surface of AA2024 and achieve over 90% corrosion inhibition efficiency within six days of immersion<sup>147,148</sup> (Fig. 16).

### 3.8 Other types

$\text{CO}_2$  is a universally corrosive gas, so a smart corrosion inhibitor sensitive to carbon dioxide is very necessary. Since nitrogen atoms of tertiary amine groups can reversibly bind to  $\text{CO}_2$ , a number of polymers containing tertiary amine groups have been developed, such as poly(diethylaminoethyl methacrylate) (PDEAEMA) and poly(dimethylaminoethyl methacrylate) (PDMAEMA), which are the most studied  $\text{CO}_2$ -responsive polymers. Jixing Wang *et al.*<sup>39</sup> successfully polymerized DMAEMA and developed an ethylcellulose-based coating with pH-responsive self-healing properties (Fig. 17). In a 3.5 wt%  $\text{NaCl}$  solution without  $\text{CO}_2$ , the coating loaded with thiourea@PHMs slowly releases the preservative, thereby improving the corrosion resistance of the scratch coating. What is more, in a 3.5 wt%  $\text{NaCl}$  solution with  $\text{CO}_2$ , which is more corrosive than one without  $\text{CO}_2$ , the corrosion resistance of scratch coatings with thiourea@PHMs added can be significantly improved

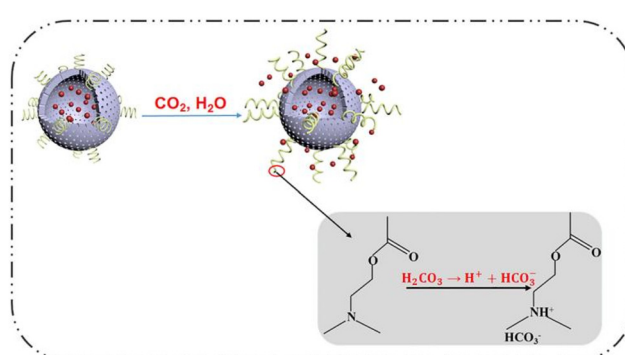
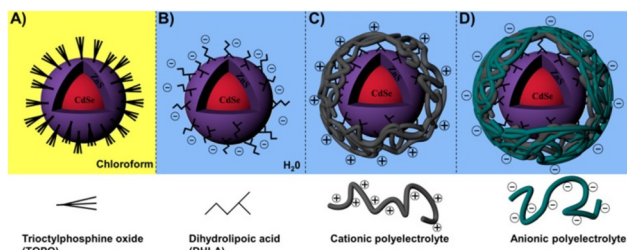


Fig. 17 Mechanism of the  $\text{CO}_2$  stimulus response. Reproduced with permission<sup>39</sup> from Elsevier.





**Fig. 18** (A) TOPO-QDs in chloroform; (B) anionic water-soluble DHLA-QDs; (C) cationic polyelectrolyte-coated quantum dots; (D) anionic polyelectrolyte-coated quantum dots. Reproduced with permission<sup>150</sup> from ACS.

because the stimulation of  $\text{CO}_2$  increases the rate of thiourea release. Much research has focused on biomedicine and controllable oil/water separation. Certain researchers have employed PDDA, PAH, and PSS as the walls of the capsule, with PAH serving as the third layer to enhance the fluorescence quantity of PSS-rhodamine. During the assembly process, oligoamine II was integrated into the capsule wall as a cationic compound. The study found that the microcapsules were initially opaque to the dye in the absence of  $\text{CO}_2$  and  $\text{N}_2$ . However, after 20 minutes' exposure to  $\text{CO}_2$ , nearly all the microcapsules became transparent to the dye. In contrast, only partial effects were observed following 5 or 10 minutes of  $\text{CO}_2$  exposure.<sup>149</sup>

A novel pH-responsive luminescent microcapsule utilizing quantum dots is designed. Utilizing dihydrolipoic acid (DHLA)-stabilized quantum dots (QDs) as templates, LbL modification of the QDs was conducted with poly(acrylamide hydride) (PAH), poly(ethylenimine) (PEI) cationic polyelectrolyte, and poly(diallyldimethylammonium chloride) (PDADMAC). Additionally, anionic polyelectrolytes such as poly(acrylic acid) (PAA), poly(sodium-4-styrenesulfonate) (PSS), and polyvinyl sulfonic acid (PVSA) were employed to form PAH-DHLA-QDs. These exhibited pH-dependent luminescence in a 50 mM Tris buffer ranging from pH 3 to 9 (Fig. 18).<sup>150</sup>

## 4 Conclusions and perspectives

Smart corrosion inhibitor systems present a milestone in the development of corrosion inhibitor anti-corrosion, overcoming the shortcomings of conventional corrosion inhibitors and conventional coating anti-corrosion. In this review, we summarized recent progress on the design and application of smart corrosion inhibitor systems based on pH, light, ion, magnetism, temperature, redox reactions, and multiple responses.

There are several advantages of applying smart responsive corrosion inhibitor systems: (i) compared with ordinary corrosion inhibitors, it can achieve a targeted response, avoiding the waste of chemicals caused by aimless release; (ii) the smart corrosion inhibitor can be combined with the coating for anti-corrosion, which saves the labour cost brought by filling com-

pared with the corrosion inhibitor, and makes up for the increased maintenance cost and the transportation loss caused by the shutdown caused by the damaged coating; and (iii) personalized customization can be carried out based on the corrosion characteristics of the corrosion conditions.

In the future, smart corrosion inhibitors will have broad applications in marine engineering, aerospace, military equipment, oil and gas exploitation, water treatment, targeted transport and release of medical drugs, and so on.

Although the development prospects of smart corrosion inhibitor systems are very broad, there are still some limitations or challenges that limit their further development and practical applications, and scholars need to conduct further research. Firstly, considering the release speed and capability of smart corrosion inhibitors, they are currently ideal for use in closed systems. If the released corrosion inhibitor is continuously discharged, the concentration of the inhibitor cannot meet the requirements for forming a dense film layer, which is a limiting factor for application in open systems. Secondly, when the smart corrosion inhibitor/smart corrosion inhibitor + carrier is combined with the coating, it needs to be highly compatible and cannot affect the barrier effect of the coating itself. Thirdly, current research on the performance of smart corrosion inhibitors only considers the influence of simple factors, while in practical applications, specific working conditions such as high temperature, high pressure, and concentrated salt environments need to be considered for their performance impact. Finally, in the construction of smart systems, it is necessary to consider simple, stable, and safe synthesis methods as well as economic issues. Moreover, it should become popular to incorporate artificial intelligence to the design of smart inhibitor system.

## Conflicts of interest

There are no conflicts to declare.

## Acknowledgements

We would like to acknowledge the support by the NSFC (No. 21975205, 21504068), Key Research and Development Program of Shaanxi (2024GX-YBXM-383), Shaanxi Academy of Fundamental Sciences (Chemistry and Biology, 23JHQ086) and Open Project of State Key Laboratory of Supramolecular Structure and Materials (sklssm2024033). We also appreciate the funding support from the College Students' Innovative Entrepreneurial Training Plan Program.

## References

- 1 A. A. Al-Amiery, W. Isahak and W. K. Al-Azzawi, *Lubricants*, 2023, **11**, 174.
- 2 M. Wasim and M. B. B. Djukic, *J. Nat. Gas Sci. Eng.*, 2022, **100**, 104467.



3 Y. Ding, X. W. Ye, H. Zhang and X. S. Zhang, *Steel Compos. Struct.*, 2024, **50**, 363–374.

4 M. Finsgar and J. Jackson, *Corros. Sci.*, 2014, **86**, 17–41.

5 X. Y. Wang, S. Liu, J. Yan, J. P. Zhang, Q. Y. Zhang and Y. Yan, *Materials*, 2023, **16**, 2954.

6 S. Liu, J. Yan, J. Q. Shi, X. Z. Li, J. P. Zhang, X. Y. Wang, N. J. Cai, Q. H. Fang, Q. Y. Zhang and Y. Yan, *Polym. Chem.*, 2023, **14**, 330–342.

7 J. Yan, X. Z. Li, X. Zhang, S. Liu, F. L. Zhong, J. P. Zhang, Q. Y. Zhang and Y. Yan, *ACS Appl. Polym. Mater.*, 2022, **4**, 3844–3854.

8 M. F. Montemor, *Surf. Coat. Technol.*, 2014, **258**, 17–37.

9 F. Zhang, P. F. Ju, M. Q. Pan, D. W. Zhang, Y. Huang, G. L. Li and X. G. Li, *Corros. Sci.*, 2018, **144**, 74–88.

10 H. Cai, P. Wang and D. Zhang, *J. Oceanol. Limnol.*, 2020, **38**, 1045–1063.

11 A. Stankiewicz, I. Szczygiel and B. Szczygiel, *J. Mater. Sci.*, 2013, **48**, 8041–8051.

12 Y. Le, P. Hou, J. Wang and J.-F. Chen, *Mater. Chem. Phys.*, 2010, **120**, 351–355.

13 E. Abdullayev, R. Price, D. Shchukin and Y. Lvov, *ACS Appl. Mater. Interfaces*, 2009, **1**, 1437–1443.

14 Z. Zheng, X. Huang, M. Schenderlein, D. Borisova, R. Cao, H. Möhwald and D. Shchukin, *Adv. Funct. Mater.*, 2013, **23**, 3307–3314.

15 A. H. Jafari, S. M. A. Hosseini and E. Jamalizadeh, *Electrochim. Acta*, 2010, **55**, 9004–9009.

16 A. Khajouei, E. Jamalizadeh and S. M. A. Hosseini, *Anti-Corros. Methods Mater.*, 2015, **62**, 88–94.

17 J. Y. Yap, S. Mat Yaakob, N. E. Rabat, M. R. Shamsuddin and Z. Man, *RSC Adv.*, 2020, **10**, 13174–13184.

18 M. Yeganeh, M. Saremi and H. Rezaeyan, *Prog. Org. Coat.*, 2014, **77**, 1428–1435.

19 M. Yeganeh and M. Saremi, *Prog. Org. Coat.*, 2015, **79**, 25–30.

20 C. J. Ward, M. DeWitt and E. W. Davis, in *Nanomaterials for Biomedicine*, 2012, pp. 209–238, DOI: [10.1021/bk-2012-1119.ch010](https://doi.org/10.1021/bk-2012-1119.ch010).

21 M. L. Zheludkevich, J. Tedim and M. G. S. Ferreira, *Electrochim. Acta*, 2012, **82**, 314–323.

22 A. B. M. da Cunha, D. A. Leal, L. R. L. Santos, I. C. Riegel-Vidotti and C. E. B. Marino, *Surf. Coat. Technol.*, 2020, **402**, 126338.

23 T. Matsuda, K. B. Kashi, K. Fushimi and V. J. Gelling, *Corros. Sci.*, 2019, **148**, 188–197.

24 K. E. Broaders, S. J. Pastine, S. Grandhe and J. M. Frechet, *Chem. Commun.*, 2011, **47**, 665–667.

25 D. I. Njoku, M. Cui, H. Xiao, B. Shang and Y. Li, *Sci. Rep.*, 2017, **7**, 15597.

26 A. Khan, A. Hassanein, S. Habib, M. Nawaz, R. A. Shakoor and R. Kahraman, *ACS Appl. Mater. Interfaces*, 2020, **12**, 37571–37584.

27 F. Olivier, R. Castaldo, M. Cocca, G. Gentile and M. Lavorgna, *ACS Appl. Mater. Interfaces*, 2021, **13**, 48141–48152.

28 A. S. Najibzad, R. Amini, M. Rostami, P. Kardar and M. Fedel, *Prog. Org. Coat.*, 2020, **140**, 105504.

29 Y. Jin, H. Duan, S. Zhan, J. Tu, T. Yang, W. Zhang, L. Ma, H. Yu and D. Jia, *ACS Appl. Mater. Interfaces*, 2023, **15**, 52971–52983.

30 A. Khan, A. Hassanein, S. Habib, M. Nawaz, R. A. Shakoor and R. Kahraman, *ACS Appl. Mater. Interfaces*, 2020, **12**, 37571–37584.

31 M. Ghaderi, A. R. SaadatAbadi, M. Mahdavian and S. A. Haddadi, *Langmuir*, 2022, **38**, 11707–11723.

32 B. Qian, Z. Zheng, M. Michailidis, N. Fleck, M. Bilton, Y. Song, G. Li and D. Shchukin, *ACS Appl. Mater. Interfaces*, 2019, **11**, 10283–10291.

33 C. Liu, B. Qian, P. Hou and Z. Song, *ACS Appl. Mater. Interfaces*, 2021, **13**, 4429–4441.

34 K. Thongchaiwetcharat, S. Salaluk, D. Crespy, H. Therien-Aubin and K. Landfester, *ACS Appl. Mater. Interfaces*, 2020, **12**, 42129–42139.

35 E. V. Skorb, D. V. Sviridov, H. Mohwald and D. G. Shchukin, *Chem. Commun.*, 2009, 6041–6043, DOI: [10.1039/b914257f](https://doi.org/10.1039/b914257f).

36 A. G. S. Ekaterina, V. Skorb, D. V. Sviridov, D. G. Shchukin and H. Möhwald, *ACS Nano*, 2009, **3**, 1753–1760.

37 J. Li and R. Buchheit, *Prog. Org. Coat.*, 2017, **104**, 210–216.

38 W. Wang, W. Li, W. Fan, X. Zhang, L. Song, C. Xiong, X. Gao and X. Liu, *Chem. Eng. J.*, 2018, **332**, 658–670.

39 J. Wang, J. Tang, H. Zhang, Y. Wang, H. Wang, B. Lin, J. Hou and H. Zhang, *Corros. Sci.*, 2021, **180**, 109194.

40 N. Y. Abu-Thabit and A. S. Hamdy, *Surf. Coat. Technol.*, 2015, 406–424.

41 M. Samadzadeh, S. H. Boura, M. Peikari, S. M. Kasiriha and A. Ashrafi, *Prog. Org. Coat.*, 2010, **68**, 159–164.

42 J. L. C. Rowsell and O. M. Yaghi, *Microporous Mesoporous Mater.*, 2004, **73**, 3–14.

43 L. Guo, C. Verma and D. Zhang, *Eco-Friendly Corrosion Inhibitors: Principles, Designing and Applications*, Elsevier, 1st edn, 2022.

44 S. Liu, J. Yan, J. Shi, X. Li, J. Zhang, X. Wang, N. Cai, Q. Fang, Q. Zhang and Y. Yan, *Polym. Chem.*, 2023, **14**, 330–342.

45 J. Yan, X. Zhang, P. Xu, J. Zhang, X. Li, F. Zhong, Y. Xu, Q. Zhang, Y. Zhu and Y. Yan, *Adv. Mater. Technol.*, 2024, 2401559, DOI: [10.1002/admt.202401559](https://doi.org/10.1002/admt.202401559).

46 J. Yan, X. Li, X. Zhang, S. Liu, F. Zhong, J. Zhang, Q. Zhang and Y. Yan, *ACS Appl. Polym. Mater.*, 2022, **4**, 3844–3854.

47 X. Wang, S. Liu, J. Yan, J. Zhang, Q. Zhang and Y. Yan, *Materials*, 2023, **16**, 2954.

48 C. Ye, O. Shchepelina, R. Calabrese, I. Drachuk, D. L. Kaplan and V. V. Tsukruk, *Biomacromolecules*, 2011, **12**, 4319–4325.

49 M. Ghidiu, J. Halim, S. Kota, D. Bish, Y. Gogotsi and M. W. Barsoum, *Chem. Mater.*, 2016, **28**, 3507–3514.

50 S. A. Haddadi, S. Hu, S. Ghaderi, A. Ghanbari, M. Ahmadipour, S. Y. Pung, S. Li, M. Feilizadeh and M. Arjmand, *ACS Appl. Mater. Interfaces*, 2021, **13**, 42074–42093.



51 N. Dararatana, F. Seidi and D. Crespy, *ACS Appl. Mater. Interfaces*, 2018, **10**, 20876–20883.

52 K. Katagiri, K. Koumoto, S. Iseya, M. Sakai, A. Matsuda and F. Caruso, *Chem. Mater.*, 2009, **21**, 195–197.

53 A. G. Skirtach, A. A. Antipov, D. G. Shchukin and G. B. Sukhorukov, *Langmuir*, 2004, **20**, 6988–6992.

54 B. Radt, T. A. Smith and F. Caruso, *Adv. Mater.*, 2004, **16**, 2184–2189.

55 P. K. Andre, G. Skirtach, M. F. Bédard, G. B. Sukhorukov and H. Möhwald, *J. Am. Chem. Soc.*, 2008, **130**, 11572–11573.

56 A. G. Skirtach, C. Dejugnat, D. Braun, A. S. Susha, A. L. Rogach, W. J. Parak, H. Möhwald and G. B. Sukhorukov, *Nano Lett.*, 2005, **5**, 1371–1377.

57 M. Bédard, A. G. Skirtach and G. B. Sukhorukov, *Macromol. Rapid Commun.*, 2007, **28**, 1517–1521.

58 K. Katagiri, A. Matsuda and F. Caruso, *Macromolecules*, 2006, **39**, 8067–8074.

59 W. Xu, I. Choi, F. A. Plamper, C. V. Synatschke, A. H. E. Müller and V. V. Tsukruk, *ACS Nano*, 2012, **7**, 598–613.

60 M. F. Bédard, S. Sadasivan, G. B. Sukhorukov and A. Skirtach, *J. Mater. Chem.*, 2009, **19**, 2226–2233.

61 R. G. Buchheit, H. Guan, S. Mahajanam and F. Wong, *Prog. Org. Coat.*, 2003, **47**, 174–182.

62 X. Guo, F. Zhang, D. G. Evans and X. Duan, *Chem. Commun.*, 2010, **46**, 5197–5210.

63 G. W. H. N. McMurray, *Corros. Sci.*, 2004, **60**, 219–228.

64 J. M. Vega, N. Granizo, D. de la Fuente, J. Simancas and M. Morcillo, *Prog. Org. Coat.*, 2011, **70**, 213–219.

65 M. L. Zheludkevich, S. K. Poznyak, L. M. Rodrigues, D. Raps, T. Hack, L. F. Dick, T. Nunes and M. G. S. Ferreira, *Corros. Sci.*, 2010, **52**, 602–611.

66 J. Tedim, S. K. Poznyak, A. Kuznetsova, D. Raps, T. Hack, M. L. Zheludkevich and M. G. Ferreira, *ACS Appl. Mater. Interfaces*, 2010, **2**, 1528–1535.

67 A. R. Aamir, I. Khan, B. Fong, C. Markland, M. O'Brien, G. R. W. Thomas, G. Dunbar and D. O'Hare, *Ind. Eng. Chem. Res.*, 2009, **48**, 10196–10205.

68 A. N. Ay, B. Zumreoglu-Karan, A. Temel and V. Rives, *Inorg. Chem.*, 2009, **48**, 8871–8877.

69 P. Gunawan, R. Xu, H. Curtius, C. Walther, K. Dardenne, K. Ufer and T. Fanghanel, *J. Phys. Chem. C*, 2009, **113**, 17206–17214.

70 T. Stumpf, H. Curtius, C. Walther, K. Dardenne, K. Ufer and T. Fanghanel, *Environ. Sci. Technol.*, 2007, **41**, 3186–3191.

71 S. L. Wang, R. J. Hseu, R. R. Chang, P. N. Chiang, J. H. Chen and Y. M. Tzou, *Colloids Surf. A*, 2006, **277**, 8–14.

72 L. C. Hsu, S. L. Wang, Y. M. Tzou, C. F. Lin and J. H. Chen, *J. Hazard. Mater.*, 2007, **142**, 242–249.

73 X. Yu, J. Wang, M. Zhang, L. Yang, J. Li, P. Yang and D. Cao, *Surf. Coat. Technol.*, 2008, **203**, 250–255.

74 C. Ding, J. Xu, L. Tong, G. Gong, W. Jiang and J. Fu, *ACS Appl. Mater. Interfaces*, 2017, **9**, 21034–21047.

75 D. Borisova, H. Möhwald and D. G. Shchukin, *ACS Nano*, 2011, **5**, 1939–1946.

76 D. V. Andreeva, E. V. Skorb and D. G. Shchukin, *ACS Appl. Mater. Interfaces*, 2010, **2**, 1954–1962.

77 M. L. Zheludkevich, D. G. Shchukin, K. A. Yasakau, H. Möhwald and M. G. S. Ferreira, *Chem. Mater.*, 2007, **19**, 402–411.

78 J. Liu, S. Z. Qiao, Q. H. Hu and G. Q (Max). Lu, *Small*, 2011, **7**, 425–443.

79 Y. Zhao, R. Berger, K. Landfester and D. Crespy, *Small*, 2015, **11**, 2995–2999.

80 S. Gu, H. Shi, C. Zhang, W. Wang, F. Liu and E.-H. Han, *Prog. Org. Coat.*, 2021, **158**, 106376.

81 R. Ghamsarizade, A. A. Sarabi, Sh. Roshan and H. E. Mohammadloo, *Colloids Surf. A*, 2022, **644**, 128883.

82 M. Alizadeh and A. Sarabi, *Prog. Org. Coat.*, 2019, **134**, 78–90.

83 P. Ghahremani, A. A. Sarabi and S. Roshan, *Surf. Coat. Technol.*, 2021, **427**, 127820.

84 G. R. Argade, S. Sanders, G. Mohandass, A. Alsaleh, F. D'Souza, T. D. Golden and R. S. Mishra, *J. Mater. Eng. Perform.*, 2019, **28**, 852–862.

85 Y. Feng, S. Chen and Y. F. Cheng, *J. Mater. Sci.*, 2017, **52**, 8576–8590.

86 T. Mauser, C. Déjugnat and G. B. Sukhorukov, *Macromol. Rapid Commun.*, 2004, **25**, 1781–1785.

87 D. V. Andreeva, D. Fix, H. Mohwald and D. G. Shchukin, *Adv. Mater.*, 2008, **20**, 2789–2794.

88 M. L. Zheludkevich, D. G. Shchukin, K. A. Yasakau, H. Möhwald and M. G. S. Ferreira, *Chem. Mater.*, 2007, **19**, 402–411.

89 T. Matsuda, N. Jadhav, K. B. Kashi, M. Jensen and V. J. Gelling, *Prog. Org. Coat.*, 2019, **132**, 9–14.

90 Z. Tan, S. Wang, Z. Hu, W. Chen, Z. Qu, C. Xu, Q. Zhang, K. Wu, J. Shi and M. Lu, *Ind. Eng. Chem. Res.*, 2020, **59**, 2657–2666.

91 J. Ress, U. Martin, J. Bosch and D. M. Bastidas, *ACS Appl. Mater. Interfaces*, 2020, **12**, 46686–46700.

92 M. Wang, J. Wang and W. Hu, *Prog. Org. Coat.*, 2020, **139**, 105434.

93 X. Xing, J. Wang, Q. Li, W. Hu and J. Yuan, *Colloids Surf. A*, 2018, **553**, 295–304.

94 X. Xing, X. Xu, J. Wang and W. Hu, *Chem. Phys. Lett.*, 2019, **718**, 69–73.

95 T. Chen and J. Fu, *Nanotechnology*, 2012, **23**, 235605.

96 F. Olivieri, F. Scherillo, R. Castaldo, M. Cocca, A. Squillace, G. Gentile and M. Lavorgna, *ACS Appl. Polym. Mater.*, 2023, **5**, 5917–5925.

97 L. R. L. Santos, C. E. B. Marino and I. C. Riegel-Vidotti, *Eur. Polym. J.*, 2019, **115**, 86–98.

98 A. Chenan, S. Ramya, R. P. George and U. Kamachi Mudali, *Ceram. Int.*, 2014, **40**, 10457–10463.

99 Y. Jia, T. Qiu, L. Guo, J. Ye, L. He and X. Li, *Appl. Surf. Sci.*, 2020, **504**, 144496.

100 S. A. Haddadi, S. A. A. Ramazani, M. Mahdavian, P. Taheri and J. M. C. Mol, *Chem. Eng. J.*, 2018, **352**, 909–922.



101 Z. Mohammadpour and H. R. Zare, *Cryst. Growth Des.*, 2021, **21**, 3954–3966.

102 K. Wei, Y. Wei, Y. Zhang, V. Kasneryk, M. Serdechnova, H. Wang, Z. Zhang, Y. Yuan, C. Blawert, M. L. Zheludkevich and F. Chen, *Corros. Sci.*, 2024, **227**, 111731.

103 M. Motamedi, S. Mohammadkhah, M. Ramezanzadeh, H. E. Mohammadloo and B. Ramezanzadeh, *ACS Appl. Mater. Interfaces*, 2022, **14**, 31170–31193.

104 D. Borisova, H. Möhwald and D. G. Shchukin, *ACS Nano*, 2011, **5**, 1939–1946.

105 J. Bao, H. Zhang, X. Zhao and J. Deng, *Chem. Eng. J.*, 2018, **341**, 146–156.

106 A. M. G. Catherine, J. Murphy, S. E. Hunyadi and C. J. Orendorff, *Inorg. Chem.*, 2006, **45**, 7544–7554.

107 C. J. Murphy, T. K. Sau, A. M. Gole, C. J. Orendorff, J. Gao, L. Gou, S. E. Hunyadi and T. Li, *J. Phys. Chem. B*, 2005, **109**, 13857–13870.

108 M. F. Bédard, D. Braun, G. B. Sukhorukov and A. G. Skirtach, *ACS Nano*, 2008, **2**, 1807–1816.

109 C. Lu, H. Möhwald and A. Fery, *J. Phys. Chem. C*, 2007, **111**, 10082–10087.

110 M. F. Bedard, B. G. De Geest, A. G. Skirtach, H. Möhwald and G. B. Sukhorukov, *Adv. Colloid Interface Sci.*, 2010, **158**, 2–14.

111 B. G. De Geest, A. G. Skirtach, T. R. M. De Beer, G. B. Sukhorukov, L. Bracke, W. R. G. Baeyens, J. Demeester and S. C. De Smedt, *Macromol. Rapid Commun.*, 2007, **28**, 88–95.

112 D. V. Volodkin, A. G. Skirtach and H. Möhwald, *Angew. Chem., Int. Ed.*, 2009, **48**, 1807–1809.

113 J. Kim, H. J. Lim, Y. K. Hwang, H. Woo, J. W. Kim and K. Char, *Langmuir*, 2012, **28**, 11899–11905.

114 X. He, C. Chiu, M. J. Esmacher and H. Liang, *Surf. Coat. Technol.*, 2013, **237**, 320–327.

115 W. Xiong, J. Tang, G. Zhu, N. Han, E. Schlangen, B. Dong, X. Wang and F. Xing, *Sci. Rep.*, 2015, **5**, 10866.

116 H. Cai, P. Wang, X. Chen, Y. Wang and D. Zhang, *Corros. Sci.*, 2020, **167**, 108534.

117 J. Li, N. Birbilis and R. G. Buchheit, *Corros. Sci.*, 2015, **101**, 155–164.

118 J. Li, B. Hurley and R. Buchheit, *Corrosion*, 2016, **72**, 1281–1291.

119 C. Motte, M. Poelman, A. Roobroeck, M. Fedel, F. Deflorian and M. G. Olivier, *Prog. Org. Coat.*, 2012, **74**, 326–333.

120 A. Ghazi, E. Ghasemi, M. Mahdavian, B. Ramezanzadeh and M. Rostami, *Corros. Sci.*, 2015, **94**, 207–217.

121 G. Williams, H. N. McMurray and M. J. Loveridge, *Electrochim. Acta*, 2010, **55**, 1740–1748.

122 A. A. Aghzzaf, B. Rhouta, E. Rocca, A. Khalil and J. Steinmetz, *Corros. Sci.*, 2014, **80**, 46–52.

123 S. P. V. Mahajanam and R. G. Buchheit, *Corrosion*, 2008, **64**, 230–240.

124 D. Li, F. Wang, X. Yu, J. Wang, Q. Liu, P. Yang, Y. He, Y. Wang and M. Zhang, *Prog. Org. Coat.*, 2011, **71**, 302–309.

125 A.-H. Lu, E. L. Salabas and F. Schüth, *Angew. Chem., Int. Ed.*, 2007, **46**, 1222–1244.

126 S. Shylesh, V. Schunemann and W. R. Thiel, *Angew. Chem., Int. Ed.*, 2010, **49**, 3428–3459.

127 A.-H. Lu and F. Schüth, *Adv. Mater.*, 2006, **18**, 1793–1805.

128 Y. W. A. D. Zhao, *Chem. Rev.*, 2007, **107**, 2821–2860.

129 F. Hoffmann and M. Fröba, *Angew. Chem., Int. Ed.*, 2006, **45**, 3216–3251.

130 Q. Yang, J. Liu, L. Zhang and C. Li, *J. Mater. Chem.*, 2009, **19**, 1945–1955.

131 Z. Lu, M. D. Prouty, Z. Guo, V. O. Golub, C. S. S. R. Kumar and Y. M. Lvov, *Langmuir*, 2005, **21**, 2042–2050.

132 S. A. Corr, Y. K. Gun'ko, R. Tekoriute, C. J. Meledandri and D. F. Brougham, *J. Phys. Chem. C*, 2008, **112**, 13324–13327.

133 K. Köhler, H. Möhwald and G. B. Sukhorukov, *J. Phys. Chem. B*, 2006, **110**, 24002–24010.

134 G. L. Li, Z. Zheng, H. Möhwald and D. G. Shchukin, *ACS Nano*, 2013, **7**, 2470–2478.

135 A. Vimalanandan, L. P. Lv, T. H. Tran, K. Landfester, D. Crespy and M. Rohwerder, *Adv. Mater.*, 2013, **25**, 6980–6984.

136 Q. Yi, D. Wen and G. B. Sukhorukov, *Langmuir*, 2012, **28**, 10822–10829.

137 P. Srikamut, T. Phakkeeree, F. Seidi, S. Iamsaard and D. Crespy, *ACS Appl. Polym. Mater.*, 2021, **3**, 5425–5433.

138 Z. Chen, X. Li, B. Gong, N. Scharnagl, M. L. Zheludkevich, H. Ying and W. Yang, *ACS Appl. Mater. Interfaces*, 2023, **15**, 2067–2076.

139 T. Siva, K. Kandhasamy, K. Vaduganathan, S. Sathiyaranayanan and A. Ramadoss, *Ind. Eng. Chem. Res.*, 2023, **62**, 3942–3951.

140 K. R. L. Castagno, V. Dalmoro and D. S. Azambuja, *Mater. Chem. Phys.*, 2011, **130**, 721–726.

141 E. N. Jun Ge, T. J. Cahill III, R. E. Beygui and R. N. Zare, *ACS Nano*, 2012, **6**, 227–233.

142 L. P. Lv, Y. Zhao, N. Vilbrandt, M. Gallei, A. Vimalanandan, M. Rohwerder, K. Landfester and D. Crespy, *J. Am. Chem. Soc.*, 2013, **135**, 14198–14205.

143 Y. Yu, Y. Zhang, Z. Jiang, X. Zhang, H. Zhang and X. Wang, *Langmuir*, 2009, **25**, 10002–10006.

144 Y. Chen, Q. Meng, M. Wu, S. Wang, P. Xu, H. Chen, Y. Li, L. Zhang, L. Wang and J. Shi, *J. Am. Chem. Soc.*, 2014, **136**, 16326–16334.

145 C. Li, X. Zhao, C. Meng, T. Zhang, S. Sun and S. Hu, *Prog. Org. Coat.*, 2021, **159**, 106437.

146 A. A. Antipov, G. B. Sukhorukov, S. Leporatti, I. L. Radtchenko, E. Donath and H. Möhwald, *Colloids Surf., A*, 2002, **198–200**, 535–541.

147 B. Li, D. Njuko, M. Meng, A. Tang and Y. Li, *ACS Appl. Mater. Interfaces*, 2022, **14**, 53370–53379.

148 T. S. Vo, T. T. B. C. Vo, T. T. Tran and N. D. Pham, *Prog. Nat. Sci.: Mater.*, 2022, **32**, 54–62.

149 L. Hartmann, M. Bedard, H. G. Borner, H. Möhwald, G. B. Sukhorukov and M. Antonietti, *Soft Matter*, 2008, **4**, 534–539.

150 A. S. Ashvin, T. Nagaraja, K. E. Meissner and M. J. McShane, *ACS Nano*, 2013, **7**, 6194–6202.

